Genomic insights into the Archaea inhabiting an Australian radioactive legacy site

Xabier Vázquez-Campos[1*], Andrew S. Kinsela[2], Mark W. Bligh[2], Timothy E. Payne[3], Marc R. Wilkins[1] & T. David Waite[2*]

[1] NSW Systems Biology Initiative, School of Biotechnology and Biomolecular Sciences, The University of New South Wales, Sydney, New South Wales 2052, Australia

[2] UNSW Water Research Centre and School of Civil and Environmental Engineering, The University of New South Wales, Sydney, New South Wales 2052, Australia

[3] Environmental Research Theme, Australian Nuclear Science and Technology Organisation, Locked Bag 2001, Kirrawee DC, New South Wales 2232, Australia

* Corresponding authors:

Running title: Archaea from Little Forest Legacy Site

Abstract

During the 1960s, small quantities of radioactive materials were co-disposed with chemical waste at the Little Forest Legacy Site (LFLS, Sydney, Australia). The microbial function and population dynamics in a waste trench during a rainfall event have been previously investigated using shotgun metagenomics. This revealed a broad abundance of candidate and potentially undescribed taxa in this iron-rich, radionuclide-contaminated environment.

Here, applying genome-based metagenomic methods, we recovered 37 refined archaeal MAGs (≥50% completeness, ≤10% redundancy) from 10 different major lineages. They were, mainly, included in four DPANN lineages without standing nomenclature (LFWA-I to IV) and *Methanoperedenaceae* (ANME-2D).

While most of the new DPANN lineages show reduced genomes with limited central metabolism typical of other DPANN, the orders under the LFWA-III lineage, '*Ca.* Gugararchaeales' and '*Ca.* Anstonellales', may constitute distinct orders with a more comprehensive central metabolism and anabolic capabilities within the *Micrarchaeota* phylum.

The new *Methanoperedens* spp. MAGs, together with previously published data, suggests metal ions as the ancestral electron acceptors during the anaerobic oxidation of methane while the respiration of nitrate/nitrite via molybdopterin oxidoreductases would have been a secondary acquisition. The presence of genes for the biosynthesis of polyhydroxyalkanoates in most *Methanoperedens* also appears to be a widespread characteristic of the genus for carbon accumulation.

We formally propose 22 new candidate taxa based on data analysed in this manuscript, as well as four missing formal taxa definitions and two new candidate species based on extant data.

We present evidence of four new DPANN lineages and six non-conspecific *Methanoperedens*, while exploring their uniqueness, potential role in elemental cycling, and evolutionary history.

Keywords: Archaea, DPANN, metagenomics, genomics, phylogenomics, ANME-2d, radionuclides

Introduction

The Little Forest Legacy Site (LFLS) is a low-level radioactive waste disposal site in Australia that was active between 1960 and 1968. During this period, small quantities of both short and long-lived radionuclides (including plutonium and americium) were disposed of in three-metre deep, unlined trenches, and covered with a shallow (1 m layer) of local soil, as was common practice at the time (Payne, 2012). Since its closure, the periodic occurrence of intense rainfall events leads to the filling of the former trenches with surface waters, which, depending on preceding conditions, can result in the trench water discharging into the surface and near-surface soils in a 'bath-tub'-like mechanism (Payne et al., 2013, 2020). Aside from providing a mechanism enabling the export of contaminants from the legacy trenches (Payne et al., 2013), the periodic influx of oxic waters into these natural reducing zones results in transitory microbial population shifts associated with pronounced elemental cycling (Vázquez-Campos et al., 2017; Kinsela et al., 2021). Our previous research showed that the archaeal community in the LFLS waste trenches, while constituting a minor portion of the whole microbial community, included a number of potentially interesting members, either in terms of phylogeny and/or functionality (Vázquez-Campos et al., 2017).

The domain Archaea constitutes by far the most understudied domain of life. Archaea have been traditionally regarded as biological oddities and marginal contributors to the global geochemical elemental cycles, with most living in extreme environments (Dombrowski et al., 2019). However, the continuous development of cultivation-independent techniques in recent decades has completely changed this perception. For example, *Thaumarchaeota* Archaea are now known to be key components in the global nitrogen cycle (Kitzinger et al., 2019) and can even induce systemic resistance to pathogens in plants (Song et al., 2019). Some *Euryarchaeota*, which are capable of the anaerobic oxidation of methane (AOM), consume up

68 to 80–90% of the methane produced in environments such as rice fields and ocean floors before
69 this highly deleterious greenhouse gas can be released into the atmosphere (Reeburgh, 2007).

70 The DPANN Archaea, so-named from its constituent lineages when it was defined
71 (*Diapherotrites*, *Parvarchaeota*, *Aenigmarchaeota*, *Nanohaloarchaeota* and *Nanoarchaeota*)
72 (Rinke et al., 2013), is an archaeal superphylum generally characterised by the small size of its
73 members (excluding *Altiarchaeota*). Their diminutiveness not only relates to their reduced
74 physical size, many of which are capable of passing through a standard 0.2 µm filter (Luef et
75 al., 2015), but also due to their small genome sizes, i.e. many are below 1 Mbp and with an
76 estimated maxima of ~1.5 Mbp. Many of the DPANN with extremely reduced genomes lack
77 biosynthetic pathways for amino acids, nucleotides, vitamins, and cofactors, which aligns with
78 a host-dependent lifestyle. Others, towards the higher end of the genome size scale, typically
79 encode for some or most of the aforementioned pathways and are regarded as free-living.
80 Irrespective of size, only a limited number of organisms from this lineage have been studied in
81 detail (Waters et al., 2003; Baker et al., 2006; Castelle et al., 2015; Youssef et al., 2015;
82 Golyshina et al., 2017).

83 Another Archaea taxon that has attracted substantial attention during the last few years are the
84 anaerobic methane oxidisers ANME-2d (Mills et al., 2003) or AAA (AOM-associated
85 Archaea) (Knittel and Boetius, 2009), now referred to as '*Ca.* Methanoperedens' (simply
86 *Methanoperedens* henceforth). These archaea have been purported to couple the oxidation of
87 methane, at its source, with the reduction of nitrate (Haroon et al., 2013), nitrite (Arshad et al.,
88 2015), Fe(III) (Ettwig et al., 2016; Cai et al., 2018), Mn(IV) (Ettwig et al., 2016) or even Cr(VI)
89 (Lu et al., 2016), constituting an important environmental pathway in mitigating the release of
90 methane into the atmosphere upon a global scale.

91 Here we describe the results from the analysis of 37 new archaeal MAGs with different degrees
92 of completeness, derived from samples collected in a legacy radioactive waste trench at the
93 LFLS during a redox cycling event. We formally propose 22 new candidate taxa based on data
94 analysed in this manuscript, as well as four missing formal taxa definitions and two new
95 candidate species based on extant data. We present evidence of four new DPANN lineages and
96 six non-conspecific *Methanoperedens* sp. genomes, while exploring their uniqueness and
97 potential role in elemental cycling.

98 Material and Methods

99 Recovery and assessment of community genomes

100 QC and pre-processing of raw sequencing reads were performed with Trim Galore!
101 (http://www.bioinformatics.babraham.ac.uk/projects/trim_galore/). Co-assembly of the
102 trimmed reads from all samples was performed with MEGAHIT v1.0.2 (Li et al., 2015, 2016)
103 (--kmin-1pass --k-min 27 --k-max 127 --k-step 10).

104 Contigs >2.5kbp were binned with CONCOCT (Alneberg et al., 2014) while limiting the
105 number of clusters to 400 to avoid 'fragmentation errors', within anvi'o v2.3 (Eren et al., 2015)
106 following the metagenomics protocol as previously described. Bins of archaeal origin were
107 manually refined in anvi'o. Completeness and redundancy were estimated with anvi'o single
108 copy gene (SCG) collection, based on Rinke *et al.* (2013), as well as with CheckM v1.0.13
109 (Parks et al., 2015). In the case of CheckM, analyses were performed by both the standard
110 parameters, with automatic detection of the marker gene set, and by forcing the universal
111 Archaea marker gene collection.

112 ## Phylogenomics and phylogenetics

113 Prodigal v2.6.3 (-p meta) was used to predict proteins from the archaeal MAGs and 242
114 archaeal reference genomes (Table S1). Predicted proteins were assigned to archaeal Clusters
115 of Orthologous Groups (arCOGs) using the arNOG database of eggNOG v4.5.1 (Huerta-Cepas
116 et al., 2016) using eggNOG-mapper v0.99.2 (Huerta-Cepas et al., 2017).

117 Initial phylogenomic reconstruction was based on the 16 ribosomal proteins by Hug *et al.*
118 (2016) with the exception of rpL16 due to frequent misannotation (Laura Hug, pers. comm.)
119 (data not shown) using the Phylosift HMM profiles (Darling et al., 2014). The resulting trees
120 showed relatively poorly resolved basal branches in addition to the absence of rpL22 genes
121 from virtually all DPANN Archaea. We found this to also be the case with other known HMM
122 profile-based databases such as TIGRFAM (Haft et al., 2013). As an example, the rpL14p in
123 DPANN Archaea is often overlooked by the TIGR03673 even when the protein is present as
124 per the more suitable model defined by arCOG04095. Subsequently, we used the more up to
125 date arNOG and increased the number of phylogenetic markers to 44 universal and archaeal
126 ribosomal proteins. Markers were selected from the universal and archaeal ribosomal protein
127 list from Yutin et al. (2012) with the following criteria: i) present in a minimum of 80% of the
128 collection of reference genomes and ii) have a limited level of duplications (standard deviation
129 of copy number in genomes with given arCOG <1.25) (Table S2).

130 Ribosomal proteins were individually aligned with MAFFT-L-INS-i v7.305b (Yamada et al.,
131 2016) and concatenated. Concatenated alignment was trimmed with BMGE v1.2 (-m
132 BLOSUM30 -g 0.5) (Criscuolo and Gribaldo, 2010) based on Lazar *et al.* (2017).

133 The concatenated archaeal protein tree was constructed using the posterior mean site frequency
134 (PMSF) model (Wang et al., 2018) in IQ-TREE v1.5.5 (Nguyen et al., 2015), a faster and less
135 resource-intensive approximation to the C10–C60 mixture models (Le et al., 2008), which are

136 also a variant of Phylobayes' CAT model. Briefly, a base tree was inferred using a simpler
137 substitution model such as LG. This tree was used as the base to infer the final tree under the
138 optimum model suggested by IQ-TREE, LG+C60+F+I+G, with 1000 ultrafast bootstrap
139 replicates (Minh et al., 2013).

140 Taxonomic identity of the recovered MAGs was also evaluated with GTDB-Tk v 0.3.0
141 (Chaumeil et al., 2020) using GTDB r89 (Parks et al., 2020). The program was run with both
142 classify_wf and then with de_novo_wf in order to attain a better placement for the MAGs with
143 a limited number of closely related references (Table S3).

144 Phylogenetic placement of new taxa in the DPANN tree

145 In addition to the rp44 and GTDB-tk analyses, phylogenetic placement of the LFLS DPANN
146 was investigated with additional methods based on a dataset containing all the representative
147 genomes of DPANN from GTDB r89 (151), the 25 LFLS DPANN MAGs, and 10
148 representatives from Altiarchaeota as outgroup.

149 Three methods were used for the DPANN-specific phylogenomic analysis: i) concatenated
150 proteins; ii) partitioned analysis; and, iii) multispecies coalescence (MSC) model with
151 ASTRAL. For these, the protein sequences used for tree inference were derived from the 122
152 SCG used for the archaeal GTDB (ar122) with certain caveats, as 31 proteins were present in
153 <50% of the full dataset (186 genomes). In all cases, each marker was aligned with MAFFT-
154 L-INS-i v7.407 (Yamada et al., 2016).

155 i) Concatenated protein (dpann-cat): a concatenated MSA was generated as for the
156 rp44 dataset using MAFFT and BMGE. The tree was generated using the PSMF
157 model. Briefly, an initial tree was generated with FastTree v2.1.10 (-lg -gamma)
158 (Price et al., 2010). The best model was searched with IQ-TREE v2.1.2 for all

159 supported mixture models plus iterations of LG with C10–C60 models (Le et al.,
160 2008). The final tree was created with model LG+C60+F+I+G and 1000 ultrafast
161 bootstrap replicates (Hoang et al., 2018).

162 ii) Partitioned analysis (dpann-part): the MSA derived from the concatenated protein
163 tree was used as input where each partition was defined as per each protein. A total
164 of 91 partitions with a length of 55-749 amino acids were included in the analysis.
165 Substitution models were selected individually per partition. Support values in IQ-
166 TREE were calculated based on 1000 ultrafast bootstrap replicates with nearest
167 neighbour interchange optimisation and --sampling GENESITE.

168 iii) Supertree with ASTRAL (dpann-astral): sequences for each marker were aligned
169 with MAFFT-L-INS-i and trimmed with BMGE v1.2 with options defined above.
170 Individual ML trees were generated for each marker with IQ-TREE v2.1.2 and the
171 suggested model for each, with 1000 ultrafast bootstrap replicates with nearest
172 neighbour interchange optimisation (Hoang et al., 2018). The resulting ML trees
173 were used as input for ASTRAL-III v5.7.7 (Zhang et al., 2018). This approach was
174 also performed with untrimmed MSA.

175 In the three scenarios, the markers were derived from the 122 archaeal markers used in the
176 GTDB, with certain caveats, as 31 proteins were present in <50% of the full dataset (186
177 genomes) and therefore automatically eliminated from the concatenated and partitioned trees.

178 Other phylogenies

179 Phylogeny of NarG-like proteins was created using all proteins (416 sequences) as reference,
180 from related orthologous groups from the EggNOG database, i.e.: arCOG01497 (19),
181 ENOG4102T1R (5), ENOG4102TDC (5), ENOG4105CRU (351) and ENOG4108JIG (36).
182 Protein sequences were clustered with CD-HIT v4.6 (-c 0.9 -s 0.9 -g 1) (Li and Godzik, 2006)

183 resulting in 276 sequences. Sequences were aligned with MAFFT-L-INS-i v7.305b (Yamada
184 et al., 2016). Alignment was trimmed with BMGE v1.2 (-g 0.9 -h 1 -m BLOSUM30) (Criscuolo
185 and Gribaldo, 2010) and the tree built with IQ-TREE v1.5.5 under the recommended model
186 (LG+R10) and 10,000 ultrafast bootstrap replicates (Nguyen et al., 2015).

187 Phylogeny of LysJ/ArgD and related proteins was created using all proteins (500 sequences)
188 as reference from related orthologous groups from Swissprot. Protein sequences were clustered
189 with CD-HIT v4.6 (with default parameters) (Li and Godzik, 2006) resulting in 256
190 representative sequences. Sequences were aligned with MAFFT-L-INS-i v7.305b (Yamada et
191 al., 2016). Alignment was trimmed with BMGE v1.2 (with defaults) (Criscuolo and Gribaldo,
192 2010) and the tree built with IQ-TREE v1.5.5 under the recommended model (LG+F+I+G4)
193 and 1,000 ultrafast bootstrap replicates (Nguyen et al., 2015).

194 Functional annotation

195 In addition to arCOGs, predicted proteomes were profiled with InterProScan v5.25-64.0 (Jones
196 et al., 2014). InterProScan was run with options --disable-precalc --pathways --goterms --
197 iprlookup and using the following databases: CDD v3.16 (Marchler-Bauer et al., 2017),
198 Gene3D v4.1.0 (Lees et al., 2014), HAMAP v201701.18 (Pedruzzi et al., 2015), PANTHER
199 v11.1 (Mi et al., 2013), Pfam v31.0 (Finn et al., 2014), PIRSF v3.02 (Wu et al., 2004), PRINTS
200 v42.0 (Attwood et al., 1994), ProDom v2006.1 (Servant et al., 2002), ProSitePatterns and
201 ProSiteProfiles v20.132 (Sigrist et al., 2013), SFLD v2 (Akiva et al., 2014), SMART v7.1
202 (Letunic et al., 2015), SUPERFAMILY v1.75 (Gough et al., 2001), and TIGRFAM v15.0 (Haft
203 et al., 2013).

204 Key biogeochemical enzymes were identified based on signature hmm profiles in the
205 InterProScan output or by custom hmm profiles not integrated in databases (Anantharaman et

206 al., 2016; Dombrowski et al., 2017). Custom hmm profiles were searched with HMMER
207 v3.1b2 (-E 1e-20) (Eddy, 2011). Proteins with single HMMER matches below previously
208 established thresholds (Anantharaman et al., 2016; Dombrowski et al., 2017) were searched
209 against Swissprot and checked against the InterProScan results to reduce the incidence of false
210 negatives.

211 High-heme cytochromes (≥10 binding sites per protein) were predicted using a modified
212 motif_search.py script (https://github.com/alexherns/biotite-scripts) that uses CX(1,4)CH as
213 well as the more canonical CXXCH heme-binding motif.

214 Carbohydrate-active enzymes were searched locally with hmmscan (HMMER v3.1b2) (Eddy,
215 2011) and the --domtblout output using a CAZy-based (André et al., 2014) hmm library v5
216 from dbCAN (Yin et al., 2012). Output was parsed as recommended with the hmmscan-
217 parser.sh script.

218 Peptidases and proteases were annotated by similarity search of the predicted proteins against
219 the MEROPS database v11.0 (blastp -max_hsps 1 -evalue 1e-4 -seg yes -soft_masking true -
220 lcase_masking -max_target_seqs 1) (Rawlings et al., 2014).

221 Transporters were annotated by similarity search against the TCDB blastp -max_hsps 1 -evalue
222 1e-4 -seg yes -soft_masking true -qcov_hsp_perc 50 -lcase_masking -max_target_seqs 1
223 (database version downloaded on 12 July 2018) (Saier et al., 2014).

224 The subcellular location of the proteins was predicted with PSORTb v3.0.6 (Yu et al., 2010).

225 Prediction of tRNA and rRNA genes was performed with tRNAscan-SE 2.0 (Chan et al., 2019)
226 and Barrnap v0.9 (https://github.com/tseemann/barrnap) respectively. Total tRNAs are
227 reported based on the 20 default aminoacyl-tRNAs plus the initiator tRNA (iMet).

228 ## Genome annotation

229 Metagenome assembled genomes were annotated with Prokka v1.12 (Seemann, 2014) with the
230 --rfam option for the annotation of ncRNA genes. Annotations were imported into
231 PathwayTools v22.0 (Karp et al., 2016) for modelling. Predicted proteins from each MAG were
232 also processed with KofamScan v1.1.0 for KEGG annotation (Kanehisa et al., 2016; Aramaki
233 et al., 2020).

234 ## Multivariate analysis of DPANN genomes

235 DPANN MAGs from LFLS were compared with extant publicly available genomes based on
236 functional and compositional characteristics. In addition to the genomes in the rp44 dataset, all
237 (165) DPANN published genomes in IMG were downloaded (15 Nov 2019). Genomes from
238 rp44 and IMG were compared with MASH v2.2.2 (Ondov et al., 2016) to remove redundant
239 genomes, resulting in 133 additional DPANN genomes to be added to the dataset (Table S4).

240 Functional data included in the analysis included COG categories, PSortb predictions, TCDB,
241 MEROPS and CAZy main categories as percentage of the total proteins predicted in each
242 genome. Compositional data included the proportion of each amino acid in the predicted
243 proteome, GC content and coding density. Before analysis, all reference genomes with %C
244 <70% (based on CheckM Archaea) were removed.

245 Multivariate analysis was performed on zero-centred scaled data via Sparse Principal
246 Component Analysis (sPCA) (Shen and Huang, 2008) as implemented in the MixOmics R
247 package v6.13.21 (Rohart et al., 2017) and limiting the number of explanatory variables per
248 component to five.

Completeness of DPANN MAGs

Due to the limited completeness values obtained for DPANN genomes – even those in the literature reported to be assembled in single contigs (Table S5), four different Archaeal or prokaryotic SCG collections were examined to assess each of the constituent markers with regard to their suitability for being included as markers for reporting completeness of DPANN MAGs. In addition to the already calculated completeness based on Rinke (default in anvi'o until v5.5 – anvi'o Rinke, 162 SCG) (Eren et al., 2021) and CheckM Archaea (149 SCG), two additional SCG libraries were utilised: anvi'o Archaea76 (76 SCG - current archaeal SCG in anvi'o) (Lee, 2019), and CheckM prokaryote (56 SCG, forced prokaryote/root SCG collections from CheckM).

An initial set of DPANN genomes based on the one used for the multivariate analysis were filtered at 50%C (193 genomes) and 75%C (101 genomes) based on completeness values obtained by CheckM Archaea. All individual markers in all SCG collections were evaluated for their prevalence in each set of genomes. Redundant markers across SCG collections were also compared in order to filter potential universal SCG that might be represented by best/flawed HMM profiles. Initial marker filtering required a prevalence of >=75% across all DPANN genomes, and a prevalence within classic DPANN lineages of >50% to account for the limited number of highly complete genomes.

Pangenomic analysis

Pangenomic analysis of the found '*Ca.* Methanoperedens spp.' genomes, as well as the four nearly complete reference '*Ca.* Methanoperedens spp.' was performed with anvi'o v5.4.0 (Eren et al., 2015) following the standard pangenomics workflow (http://merenlab.org/2016/11/08/pangenomics-v2). The reference genomes included in all

272 comparisons and pangenome analysis were: '*Ca.* Methanoperedens nitroreducens' ANME-2D
273 (type genome, JMIY00000000.1) (Haroon et al., 2013), '*Ca.* Methanoperedens ferrireducens'
274 (PQAS00000000.1) (Cai et al., 2018), '*Ca.* Methanoperedens batavicum' comb. nov.
275 (previously referred to as '*Ca.* M. nitroreducens' BLZ1 or MPEBLZ) (LKCM00000000.1)
276 (Arshad et al., 2015), and '*Ca.* Methanoperedens vercellense' comb. nov. (previously '*Ca.* M.
277 nitroreducens' Vercelli, GCA_900196725.1) (Vaksmaa et al., 2017). Protein-coding genes
278 were clustered with an MCL inflation value of 6 (van Dongen and Abreu-Goodger, 2012).

279 Average Nucleotide Identity (ANI) and Average Amino acid Identity (AAI) were calculated
280 with pyani v0.2.7 (Pritchard et al., 2015) and CompareM v0.0.23
281 (https://github.com/dparks1134/CompareM) respectively.

282 Proposed taxa

283 Details on etymology and nomenclature can be found in the Taxonomic Appendix. A summary
284 of the proposed taxa can be found in Table 1.

285 Minimal quality criteria for denominating new candidate species was based on Chuvochina et
286 al. (2019). Relaxed parameters were allowed for selected genomes when
287 phylogenetic/taxonomic novelty was deemed of special relevance. Under those conditions no
288 new names were proposed even under taxonomic novelty (e.g. LFWA-IV) for MAGs with
289 completeness <90%, <18 tRNA, and/or 16S rRNA gene sequence <1000 bp. Additional details
290 about the proposed species can be found in Table S6.

Data availability

Annotated assemblies are available at ENA under project PRJEB21808 and sample identifiers ERS2655284–ERS2655320. See details in Table S7. The output of the different analyses, including the reference genomes, are available at Zenodo (doi:10.5281/zenodo.3365725).

Results

Binning results and archaeal community

In order to better understand the archaeal contributions in LFLS groundwaters and their influence upon site biogeochemistry, raw sequencing reads from ENA project PRJEB14718 (Vázquez-Campos et al., 2017) were reanalysed using genome-based metagenomic methodologies. Briefly, samples were collected in triplicate over a period of 47 days at four time-points (0, 4, 21 and 47 days) after an intense rainfall event that filled the trench. Thorough chemical and radiochemical analyses were conducted on the samples in order to fully characterise the geochemistry (Vázquez-Campos et al., 2017). Over this time period, the redox conditions transitioned from slightly oxic to increasingly reducing/anoxic, reflected in both the chemical analyses and the community profile, with a clear increase in obligate anaerobes on days 21 and 47 (Vázquez-Campos et al., 2017).

The *de novo* co-assembly of sequence reads from the LFLS trench subsurface water samples (Vázquez-Campos et al., 2017) generated 187,416 contigs with a total length of 1.32 Gbp (based on 2.5 kbp cutoff). Binning with CONCOCT generated 290 initial bins. A total of 21 bins with clear archaeal identity or with ambiguous identity (similar completeness scores for bacterial and archaeal SCG profiles) were further refined with anvi'o, producing 37 curated

312 archaeal MAGs with completeness ≥50% (%C from here on; 22 of ≥90%C) and redundancy
313 ≤10% (%R from here on) (Table 2 and Table S8 for detailed completeness assessment).

314 Phylogeny based on the 44 concatenated ribosomal proteins (rp44, Figure 1) showed that most
315 metagenome assembled genomes (MAGs) from LFLS belonged to diverse DPANN lineages
316 and *Methanomicrobia* (*Methanoperedenaceae* and *Methanotrichaceae*) (Table 2).
317 Phylogenomic analysis based on the rp44 (Figure 1) showed a general tree topology largely
318 consistent with current studies, e.g. *Asgardarchaeota* as sister lineage to TACK and
319 *Altiarchaeota* as sister to DPANN (Zaremba-Niedzwiedzka et al., 2017; Dombrowski et al.,
320 2019). Most high level branches showed UF bootstrap support values >90%, with the exception
321 of the very basal Euryarchaeota, which is known to be difficult to resolve (Adam et al., 2017).
322 The position of the MAGs in the archaeal phylogeny suggests four new lineages (Figure 1)
323 within DPANN, denoted LFWA-I to -IV. These lineages correspond to representatives of high-
324 level taxa (order or above) that do not have either a current proposed name or have not been
325 explored in detail in the literature. As a means of honouring the Australian Aboriginal
326 community, and very especially, the traditional owners of the land where LFLS is located,
327 many of the nomenclatural novelties proposed are based on terms from Aboriginal languages
328 related to the site (mainly Dharawal), see Taxonomic Appendix. A summary of the
329 nomenclatural proposals derived from this work are summarised in Table 1.

330 During the drafting of this manuscript, a genome-based taxonomy was developed for Bacteria
331 and Archaea (GTDB) (Parks et al., 2018). For all proposed lineages, we have included the
332 possible correspondence with the GTDB taxonomy (r89) wherever necessary using the GTDB
333 nomenclature with prefixes, e.g. "p__" for phylum, to avoid confusion with more "typically"
334 defined lineages with the same names.

335 ## The archaeal community in detail

336 Based on bin coverage information, the archaeal community was dominated by DPANN, esp.
337 *Pacearchaeota* and LFWA-III (see below), and *Euryarchaeota,* esp. *Methanoperedenaceae*,
338 with maximum relative abundance values of 79.7% at day 4, and 42.8% at day 47, respectively
339 (Table S9). Our previous analysis indicated that DPANN constituted a maximum of 55.8% of
340 the archaeal community (Vázquez-Campos et al., 2017). This discrepancy could be an artefact
341 derived from the different copy numbers of rRNA gene clusters, often limited to one in DPANN
342 and TACK, compared to other Archaea with more typically sized genomes containing multiple
343 copies of the operon.

344 Based on the functional annotation of key biogeochemical proteins (Figure 2 and Table S10),
345 the archaeal MAGs recovered from LFLS do not appear to play a major role in the sulfur cycle
346 (lacking dissimilatory pathways, Table S10). Regarding the nitrogen cycle, the presence of
347 nitrogenases in some of the *Methanoperedens* MAGs (Figure 2 and Table S10) suggest that
348 they may play a larger role in the fixation of N_2 than in the dissimilatory reduction of nitrate,
349 particularly given the negligible nitrate concentrations measured (Vázquez-Campos et al.,
350 2017). Another Archaea likely to be heavily involved in the nitrogen cycle, but through the
351 degradation of proteins, is the *Thermoplasmata* LFW-68_2, based on the unusually high
352 number of proteases encoded in its genome (Figure 2, Figure S1 and Table S11; see SI for
353 details).

354 Due to their special interest and relevance, the content below is focused on the new DPANN
355 and the *Methanoperedens* spp. from LFLS. Aspects related to other MAGs and other general
356 observations regarding the whole archaeal community are contained within the Supplementary
357 Materials.

358 # DPANN in Little Forest Legacy Site

359 ## LFWA-I: candidate order *Tiddalikarchaeales*

360 The LFWA-I lineage is a sister lineage to *Parvarchaeota* (ARMAN-4 and -5) (Baker et al.,
361 2006; Rinke et al., 2013) in rp44 and contains a unique MAG, LFW-252_1 ('*Ca.*
362 Tiddalikarchaeum anstoanum') (Figure 1, Figure S5). LFWA-I corresponds to the order and
363 family o__CG07-land f__CG07-land within the c__*Nanoarchaeia* as per GTDB. As with many
364 other DPANN from the PANN branch (such as cluster 2 in Dombrowski et al (2020)) %C
365 estimates with existing Archaea SCG collections are severely underestimated with barely
366 79.0%C reported by CheckM (best). The %C combined with the assembly size sets a complete
367 genome size >1.5 Mbp, well above the expected genome size for a Nanoarchaeota, and similar
368 to that for many PANN MAGs (Table S8). A dedicated SCG collection was built from extant
369 HMM profiles by removing SCG's normally absent from all DPANN and/or from specific sub-
370 lineages. This first attempt of a tailored SCG library for assessing the completeness of DPANN
371 genomes (Table S12), provides more sensible results not only for LFW-252_1
372 (95.7%C/1.1%R) but also for DPANN assemblies in general, including some well-studied
373 references (Table S5).

374 The LFW-252_1 lacks the biosynthetic capacity for almost all amino acids, and for the *de novo*
375 enzymes biosynthesising purine and pyrimidine, despite having a normal enzymatic
376 representation for interconversion of purine nucleotides, and interconversion of pyrimidine
377 nucleotides (Figure S2). With the additional lack of a proper pentose biosynthesis pathway and
378 only containing the last enzyme required for the biosynthesis of 5-phospho-α-D-ribose 1-
379 diphosphate (PRPP), LFW-252_1 is very likely to depend on a host, maybe aerobic or
380 microaerophilic, although this is only based on the relative abundance patterns. Reactive
381 oxygen species detoxification is mediated by superoxide reductase (SOR,

382 neelaredoxin/desulfoferredoxin; TIGR00332) and rubredoxin. LFW-252_1 is a subsurface
383 decomposer based on the CAZymes associated to the degradation of lignocellulosic material,
384 including carbohydrate esterases (CE1, CE12 and CE14), β-mannase (GH113), and even one
385 vanillyl-alcohol oxidase (AA4) (Figure 2, Table S13). Its genome also harbours three different
386 sialidases (GH33), at least two extracellular, making it one of the few non-pathogenic
387 prokaryotes containing this enzyme (Buelow et al., 2016). In addition to the sialic acids as
388 sources of C and N, LFW-252_1 also contains two extracellular serine peptidases (S08A,
389 subtilisin-like), indicating a possible active role in the degradation of proteins in the
390 environment (Table S11). Energy production is based on the ferredoxin-mediated oxidative
391 decarboxylation of pyruvate (PorABC), 2-oxoglutarate (KorAB), and, likely, other oxoacids
392 (OforAB), i.e. fermentation of carbohydrates and amino acids.

393 LFWA-II: candidate order *Norongarragalinales*

394 The lineage LFWA-II is represented in LFLS by MAGs LFW-144_1 and LFW-156_1, and it
395 is consistently placed as a sister clade to LFWA-III+*Micrarchaeales* (see taxonomic novelties;
396 Figure 1, Figure S2). Both MAGs have a similar size but different completeness estimates and
397 GC content: 93.5%C/1.1%R and 57.5% GC for LFW-144_1, and 90.3%C/8.6%R and 32.5%
398 GC for LFW-156_1. Each of the LFWA-II MAGs belong to different genera based on AAI,
399 and to different families within o__UBA8480 (c__*Micrarchaeia*) based on the GTDB. '*Ca.*
400 Norongarragalina meridionalis' LFW-144_1, is the most complete genome within this order
401 and co-generic with the only representative on the placeholder family f__0-14-0-20-59-11.

402 Functionally, LFW-144_1 is an auxotroph for most amino acids, displaying little capacity for
403 amino acid interconversion (Figure S3). Conversely, it carries a complete pentose-phosphate
404 pathway and a capacity for *de novo* biosynthesis of purine and pyrimidine nucleotides. While
405 it lacks extracellular CAZymes (Figure 2), it has an extracellular metallopeptidase M23B

406 (lysostaphin-like). M23 peptidases are often used to break bacterial cell walls as either a
407 defence mechanism (bacteriocin) or for nutrition (e.g. predation or parasitism). Energy
408 production is derived from the fermentation of pyruvate (PorABCD).

409 Despite the similar assembly size (<3 kbp difference) and similar %C compared to LFW-
410 144_1, LFW-156_1 presents an even more limited genome, lacking complete *de novo*
411 nucleotide biosynthesis and pentose phosphate pathways. Conversely, it has three different
412 extracellular glycoside hydrolases (GH74, GH57, GH23) and one protease (S08A). It ferments
413 D-lactate (D-lactate dehydrogenase, LDH) instead of pyruvate.

414 LFWA-III is two distinct but similar *Micrarchaeota* lineages: candidate orders 415 *Gugararchaeales* and *Anstonellales*

416 LFWA-III is the closest branch to *Micrarchaeales*, constituting a match with GTDB's
417 placeholding order o__UBA10214 within c__*Micrarchaeia* according to the GTDB-tk output.
418 The lineage LFWA-III was the most diverse of all Archaea encountered at LFLS with 10
419 MAGs belonging to three different families and 10 different genera based on AAI values and
420 phylogeny (Tables S14 and S15).

421 Phylogenetic analysis and RED values suggest though that LFWA-III is actually two similar
422 but distinct orders (Figure 3). The RED for the two possible orders (LFWA-IIIa, 0.526; and
423 LFWA-IIIb, 0.525) are closer to the median value to the RED estimates for order (0.43–0.57,
424 median 0.51) than the LFWA-III's RED (0.47). While LFWA-IIIb seems to be topologically
425 consistent across trees, LFWA-IIIa is paraphyletic in rp44 and dpann-astral. In addition, both
426 the GTDB-tk derived trees and our DPANN trees show LFWA-IIIb to be equivalent to a pre-
427 existing order in GTDB, o__UBA10214 (Figure 3).

428 LFWA-IIIa, or *Gugararchaeales*, includes three MAGs (Table 2) belonging to three different
429 families, but only two of high quality: LFW-121_3, '*Ca.* Gugararchaeum adminiculabundum'
430 LFW-121_3 (96.8%C, 2.2%R, 49.8% GC), and LFW-281_7, '*Ca.* Burarchaeum australiense'
431 LFW-281_7 (96.8%C, 5.4%R, 57.6% GC). Both MAGs constitute the types of their respective
432 families, *Gugararchaeaceae* and *Burarchaeaceae*. On the other hand, LFWA-IIIb or
433 *Anstonellales*, is the most diverse order in LFLS waters, with 7 MAGs from two different
434 families, but only two of high quality: LFW-35, '*Ca.* Anstonella stagnisolia' (97.8%C, 2.2%R,
435 62.2% GC), and LFW-283_2, '*Ca.* Bilamarchaeum dharawalense' (95.7%C, 0%R, 40.0% GC).
436 *Anstonellaceae* would be equivalent to f__UBA10161, while *Bilamarchaeaceae* would be
437 equivalent to f__UBA10214. In terms of abundance, LFWA-III, in general, constituted >25%
438 of the archaeal community at any individual sampling day with '*Ca.* Anstonella stagnisolia'
439 LFW-35 being the most abundant Archaea at day 0 and the second most abundant during the
440 remaining days (Table S9).

441 **Comparative functional analysis**

442 In addition to their high abundance and diversity, LFWA-III is also an interesting lineage at a
443 functional level, constituting one of the few DPANN with broad anabolic capabilities including
444 the *de novo* biosynthesis of the amino acids lysine, arginine, and cysteine as well as purine and
445 pyrimidine nucleotides (Figure 4). The metabolic capabilities of the top five LFWA-III
446 genomes (the four named species plus LFW-29) were compared with five of the better
447 characterised and/or complete DPANN genomes (Figure 4): '*Ca.* Iainarchaeum andersonii'
448 (Youssef et al., 2015) and AR10 (Castelle et al., 2015) (*Diapherotrites*), '*Ca.* Micrarchaeum
449 acidiphilum' ARMAN-2 (Baker et al., 2006) and '*Ca.* Mancarchaeum acidiphilum' Mia14
450 (Golyshina et al., 2017) (*Micrarchaeota*), and "*Nanoarchaeum equitans*" Kin4-M (Huber et
451 al., 2002; Waters et al., 2003) ("*Nanoarchaeota*"). In terms of core metabolism, the
452 representative genomes of LFWA-III share more similarities with *Diapherotrites* than with

453 *Micrarchaeota*, e.g. *de novo* biosynthesis pathways for nucleotides, de novo biosynthesis of
454 nicotinate/nicotinamide or aromatic amino acids (Figure 4). However, LFWA-III also contains
455 other unique features: pathways for the biosynthesis of L-arginine, L-lysine, L-cysteine, and
456 L-histidine (only in AR10 in the reference genomes). Both LFWA-IIIa MAGs display most of
457 the genes encoding the pathway for the biosynthesis of branched amino acids. Conversely, in
458 the case of LFWA-IIIb, and likely also with '*Ca.* Iainarchaeum andersonii', would likely rely
459 on the interconversion of L-valine and L-leucine. LFW-121_3 in particular presents unique
460 features that either distinguish it from other LFWA-III genomes and/or the reference genomes.
461 Both LFW-121_3 and '*Ca.* Iainarchaeum andersonii' are the only MAGs able to convert L-
462 aspartate to L-threonine based upon current evidence.

463 Another interesting difference between *Diapherotrites* and LFWA-IIIa relates to thiamine
464 acquisition (Figure 4). Both *Diapherotrites* genomes have transporters for thiamine and/or its
465 phosphorylated forms but lack any enzyme known in the *de novo* pathway for its biosynthesis.
466 Instead, LFWA-IIIa is likely to be able to produce thiamine *de novo* provided a source for the
467 thiazole branch of the thiamine pathway is available (see SI for further discussion). None of
468 the LFWA-IIIb MAGs have the biosynthetic pathway nor specific transporters for thiamine.

469 Like other DPANN, all LFWA-III are fermentative organisms. However, there are differences
470 in the substrates used. Leaving aside LFW-281_7, for which we couldn't detect any of the
471 proteins mentioned next, all other LFWA-III and ARMAN-2 can ferment 2-oxoglutarate
472 (KorAB), and other 2-oxoacids (OforAB). Pyruvate fermentation was detected in both
473 *Diapherotrites* and ARMAN-2 but not in any LFWA-III. *Anstonellaceae* MAGs (LFW-35,
474 LFW-29) were the only ones with LDH, a differential characteristic from the other LFWA-III,
475 but shared with '*Ca.* Iainarchaeum andersonii'. LFW-121_3 was the only one with a predicted

476 capacity for the fermentation of aromatic amino acids amongst the 10 genomes compared
477 (IorAB).

478 Regarding transporters (Figure 4), the high variability across individual MAGs makes
479 generalisations difficult. Nonetheless, certain types of transporters show a distinctive
480 distribution. Chloride channel proteins (TCDB 2.A.49.6.1), TCDB-2 antibiotic exporters (e.g.
481 MarC family), H^+,K^+/Na^+ antiporters and Mg^{2+} P-type ATPase (MgtA/MgtB, Mg^{2+} import)
482 appear unique to LFWA-III. Two transporters appear to be specific for LFWA-IIIa: the
483 potassium channel protein (TCDB 1.A.1.21.1) and the uncharacterised TCDB 1.B.78.1.4 now
484 annotated as a VIT family protein (TCDB 2.A.89.1.9), often involved in iron homeostasis.
485 Ca^{2+}/Na^+ and H^+/K^+ antiporters, and Ca^{2+} P-type ATPase are common to both LFWA-III and
486 *Diapherotrites*.

487 LFWA-IV: an *incertae sedis* DPANN lineage

488 The MAG LFW-46 is the sole representative of the LFWA-IV lineage (Figure 1). While
489 presenting good %C/%R levels for a functional description (92.5%C, 3.2%R, 43.8% GC), it
490 lacks all rRNA genes aside from a partial 5S (thus no name is formally proposed, Figure S3).
491 All the DPANN trees place LFW-46 as sister to EX4484-52 (member of the unnamed
492 homonym phyla) and, together, a sister to *Nanohaloarchaeota*.

493 The LFW-46 genome is a typical example of a reduced, host-dependent DPANN (Figure S4)
494 with very limited amino acid interconversion pathways, lacking both the *de novo* nucleotide
495 biosynthesis as well as the pentose phosphate pathways. However, LFW-46 differentiates itself
496 by the relatively rich repertoire of transporters related to resistance, especially in comparison
497 with the repertoire of other DPANN: multidrug, tetracycline, quinolones, arsenite, Cu^+ and
498 Cu^{2+}, and mono-/di-valent organocations (e.g. quaternary ammonium compounds). The
499 extracellular enzymes of LFW-46 include one protease (S08A), one glycoside hydrolase

500 (GH57), and one polysaccharide lyase (PL9). LFW-46 ferments pyruvate for energy
501 (PorABCD).

502 Multivariate comparison of DPANN genomes

503 Sparse Principal Component Analyses (sPCA) of the functional (e.g. COG, and MEROPS
504 annotations) and/or compositional (amino acid composition of predicted proteins, and GC%)
505 profiles of selected Archaea and DPANN genomes (only ≥75%C based on CheckM) were
506 performed in order to reveal the overall distinctiveness of LFWA lineages. In the all-Archaea
507 dataset with compositional+functional data, LFWA-III clustered closer to other DPANN
508 genomes (Figure S5) yet positioned near to what could be referred to as a 'transition zone'
509 between DPANN and normal-sized archaeal genomes (e.g. Euryarchaeota and TACK).
510 Compositional and functional analysis provided an insight into the uniqueness of LFWA-III:
511 displaying high GC% (usually ~50% or greater) and an overall above-average number of COG-
512 annotated proteins.

513 Functional sPCA of the 140 DPANN genomes enabled differentiation of the metabolically rich
514 (e.g. LFWA-II, LFWA-III, Diapherotrites and related) and acidophilic lineages from the other
515 DPANN genomes (Figures 5A and 5B). This differentiation of LFWA-III was mainly shown
516 in PC1 (Figure 5A; COG categories L, O, U, W) and PC3 (not shown; COG E, F, H and
517 MEROPS C).

518 The high positive loadings in the compositional dataset along PC1 for Gly, Ala, and GC, and
519 negative loadings for Ile and Asn may be due to the high GC content of most LFWA-III
520 genomes (Table 2, Figure 5B), considering that those amino acids are encoded by GC-rich and
521 AT-rich codons respectively (Grosjean and Westhof, 2016). Very high positive values along
522 PC2 separated the acidophilic DPANN related to the acidophilic *Micrarchaeota* and
523 *Parvarchaeota* from the other DPANN.

524 ## Diverse and abundant '*Ca.* Methanoperedens spp.'

525 The occurrence of three methanogenic MAGs from the *Methanotrichaceae* family (previously
526 indicated to be the illegitimate *Methanosaetaceae* (Vázquez-Campos et al., 2017)) were
527 principally and, unsurprisingly, detected during the highly anoxic phase (117–147 mV
528 Standard Hydrogen Electrode). More interestingly though, was the recovery of MAGs
529 belonging to the genus '*Ca.* Methanoperedens'. A total of six MAGs were assembled in this
530 study, four ≥95%C (all <10%R). Each of these MAGs belong to different species based on
531 ANI and AAI scores (Figure 6, Tables S16 and S17), constituting the most diverse set of
532 *Methanoperedens* spp. genomes reconstructed to date in a single study and site, and all different
533 to previously sequenced MAGs.

534 The rich collection of *Methanoperedens* spp. recovered, in combination with selected published
535 genomes, allows for the universal investigation of common aspects across the whole genus. A
536 total of four reference genomes are included in all comparisons and pangenome analysis: '*Ca.*
537 Methanoperedens nitroreducens' ANME-2D (Haroon et al., 2013), '*Ca.* Methanoperedens
538 ferrireducens' (Cai et al., 2018), '*Ca.* Methanoperedens batavicum' comb. nov. (previously
539 referred to as '*Ca.* M. nitroreducens' BLZ1 or MPEBLZ) (Arshad et al., 2015), and '*Ca.*
540 Methanoperedens vercellense' comb. nov. (previously '*Ca.* M. nitroreducens' Vercelli)
541 (Vaksmaa et al., 2017) (see Taxonomic appendix and SI).

542 ### Multiple acquisition of respiratory molybdopterin oxidoreductases

543 Most known *Methanoperedens* spp. encode some molybdopterin oxidoreductase enzyme,
544 which are usually referred to as NarG. All the *Methanoperedens* spp. found at LFLS share a
545 putative molybdopterin oxidoreductase not present in other members of the genus (Figure 7).
546 Notably, this is different from any canonical or putative NarG (as is often suggested for other

547 *Methanoperedens* spp.) with no match to HMM profiles characteristic of these proteins but,
548 instead, belonging to arCOG01497/TIGR03479 (DMSO reductase family type II enzyme,
549 molybdopterin subunit).

550 Phylogenetic analysis (Figure 7) places the molybdopterin oxidoreductase form of LFLS
551 *Methanoperedens* spp. far from molybdopterin oxidoreductases from the reference
552 *Methanoperedens* spp.. However, it is located closer to non-canonical NarG sequences from
553 *Haloferax mediterranei* (I3R9M9) (Lledó et al., 2004) and other *Halobacteria*, as well as to
554 the perchlorate reductase (PcrA) of *Dechloromonas aromatica* and *Azospira oryzae*
555 (previously known as *Dechlorosoma suillum* strain PS) (He et al., 2019).

556 High heme cytochromes are common in *Methanoperedens* spp. genomes

557 Metal respiration is usually associated with cytochromes with a high number of heme-binding
558 sites (≥10) or high heme cytochromes (HHC from here on). The screening of the
559 *Methanoperedens* spp. MAGs from LFLS revealed multiple HHC in all genomes, with a
560 minimum of six copies for LFW-280_1_1 (68.5%C, Figure 2, Table S10). All reference
561 *Methanoperedens* spp. genomes revealed similar abundances when considering their
562 completeness, i.e., ~10 HHC per genome. While most gene clusters containing HHC are
563 present in the cloud genome or as singletons, there is one highly conserved gene cluster in the
564 core genome (GC_00000135) of *Methanoperedens* containing 13 heme-binding sites.
565 Although metal reduction has only been confirmed for *M. ferrireducens* and *Methanoperedens*
566 *batavicum* BLZ1 (Ettwig et al., 2016; Cai et al., 2018), our data suggests metal reduction might
567 be a universal characteristic of *Methanoperedens* spp.

568 ### Biosynthesis of polyhydroxyalkanoates

569 Polyhydroxyalkanoates (PHA) are carbon-rich, energetic polymers that result from the
570 polymerisation of hydroxyalkanoates, e.g. 3-hydroxybutyrate, produced by numerous
571 microorganisms under unfavourable conditions, particularly in association with unbalanced
572 nutrient levels (Reddy et al., 2003; Martínez-Gutiérrez et al., 2018). Genes involved in the
573 biosynthesis of polyhydroxyalkanoates (PHA) were detected in three of the most complete
574 *Methanoperedens* spp. genomes, i.e. LFW-24, LFW-280_3_1 and LFW-280_3_2, as well as
575 in the *Thaumarchaeota* LFW-283_4_5 (Figure 2, Table S10).

576 In *Methanoperedens* spp., the genes associated with the biosynthesis of PHA are usually
577 present as an operon (Figure S6A). Although not explicitly reported in their respective
578 manuscripts, PhaC (PHA synthase type III heterodimeric, TIGR01836) and PhaE (PHA
579 synthase subunit E, PF09712) were predicted in all the *Methanoperedens* reference genomes
580 included in this study (Haroon et al., 2013; Arshad et al., 2015; Vaksmaa et al., 2017; Cai et
581 al., 2018). However, while all PhaC proteins form a gene cluster in the pangenome analysis,
582 PhaE does not (Figure 6). This could be related to their function: PhaC is a catalytic protein
583 while PhaE 'simply' regulates PhaC (Koller, 2019), so any sequence modifications in PhaC
584 might have a more critical effect on the biosynthesis of PHA. Both proteins, PhaC and PhaE,
585 have also been predicted in three of the most complete new genomes in the present study (LFW-
586 24, LFW-280_3_1 and LFWA-280_3_2). In most instances, PHA biosynthesis genes have
587 been found in putative operons (Figure S8A).

588 # Discussion

589 In this study we describe 22 new DPANN Archaea candidate taxa (species to order), as well as
590 proposing four supraspecific taxa to accommodate extant and newly proposed lineages

591 according to formal taxonomy (family to class), along with the proposal of two '*Ca.*
592 Methanoperedens spp.' based on extant data.

593 The archaeal community at LFLS, showed a clear dominance of DPANN and '*Ca.*
594 Methanoperedens spp.', with the data sets' uniqueness highlighted by the unmatched MAGs
595 (at species level) with any extant reference genomes. Amongst the DPANN MAGs recovered,
596 a number of them constitute the first detailed description of lineages with placeholder names
597 from large scale projects (Parks et al., 2017, 2020; Rinke et al., 2020).

598 Self-sustaining DPANN – possibly more common than previously 599 thought?

600 The DPANN archaea *sensu stricto* (i.e. not including *Altiarchaeota*) are often described as
601 organisms with extremely reduced metabolic capacities and generally, with few exceptions,
602 dependent on a host for the acquisition of essential metabolites such as vitamins, amino acids
603 or even reducing equivalents (Dombrowski et al., 2019). During the metabolic reconstruction
604 of individual archaeal genomes, it was observed that select DPANN from the LFWA-III
605 lineage, exemplified by LFW-121_3 ('*Ca.* Gugararchaeum adminiculabundum'), possess near-
606 complete pathways for the synthesis of amino acids, purine and pyrimidine nucleotides,
607 riboflavin, and thiamine (Figure 4). These predictions, derived from either Pathway Tools (via
608 Prokka annotations) or KEGG, were unusual given that when a DPANN genome lacks the
609 biosynthetic capacity for an amino acid, all enzymes for that pathway are typically missing.
610 However, several of the pathways in the *Gugararchaeales* and *Anstonellales* MAGs had a
611 limited number of gaps (Figure 4). These alleged 'gaps', thoroughly discussed in the SI with
612 focus on LFW-121_3, were often related to unusual enzymes poorly annotated in databases, or
613 steps known to be possibly performed by bifunctional or promiscuous enzymes. Manual

614 curation with predicted functions from other databases combined with literature searches was
615 able to fill some of those gaps or, at least, provide reasonable candidate proteins that may
616 perform those functions.

617 The discovery of additional DPANN taxa with a "rich" metabolism, at least compared with
618 host-dependant DPANN (e.g. "*Nanoarchaeum*", *Nanopusillus*, Mia14), highlights the
619 metabolic diversity and widespread existence of free-living DPANN *Archaea*, at least within
620 the *Diapherotrites*/*Micrarchaeota* lineage – DM branch or cluster 1 (Dombrowski et al., 2020)
621 – as opposed to the PANN branch, suggesting a more generalised genome streamlining
622 process/loss of function in the latter. Prior studies have remarked upon the generalised "limited
623 metabolic capacities" in most DPANN (Dombrowski et al., 2019). However, many DPANN
624 datasets are heavily enriched with lineages that are likely to be host-dependent, e.g.
625 *Pacearchaeota* or *Woesearchaeota* (suggested to be orders in the GTDB), or derived from
626 acidic environments, generally restricted to ARMAN lineages, esp. *Micrarchaeaceae*. This
627 study expands the phylum *Micrarchaeota* with 3 orders, 5 families, 5 genera and 5 species.
628 (Figure 3).

629 Several studies have reported that ultra-small *Bacteria* and *Archaea* can be lost using standard
630 0.22 µm filters (Luef et al., 2015; Chen et al., 2018). However, this may only affect individual
631 cells, while host-DPANN cell associations would be retained and overrepresented compared
632 to free-living DPANN, which are not necessarily larger than the host-associated organisms.
633 The high abundance of the putative free-living LFWA-III in the metagenomic samples from
634 LFLS could be related to the elevated concentrations of labile colloidal Fe that precipitates at
635 the redox interface following the infiltration of oxic-rainwaters. Acting in a similar manner as
636 a flocculant in water treatment, iron (oxyhydr)oxide microaggregates have immense capacity
637 to trap organic matter and microbial cells (Tang et al., 2016). This process has been used in

638 protocols to recover and concentrate viruses from environmental samples without the need of
639 ultrafiltration (John et al., 2011). As such, the colloidal Fe would also have improved the
640 recovery of free-living DPANNs and any other ultra-small microorganisms that, by default
641 would have been otherwise lost during the filtration with the 0.22 µm filters used during
642 sampling (Vázquez-Campos et al., 2017).

643 '*Ca.* Methanoperedens': molybdopterin oxidoreductases, metal 644 reduction and PHA biosynthesis

645 *Methanoperedenaceae* archaea have been reported (or at least suggested) to be able to utilise a
646 wide range of inorganic electron acceptors for AOM, including nitrate (Haroon et al., 2013),
647 nitrite (Arshad et al., 2015), Fe(III) (Ettwig et al., 2016; Cai et al., 2018), Mn(IV) (Ettwig et
648 al., 2016) and Cr(VI) (Lu et al., 2016). The type species of the genus *Methanoperedens*, '*Ca.*
649 Methanoperedens nitroreducens', receives its name from its ability to use nitrate as an electron
650 acceptor (Haroon et al., 2013). However, the alpha subunit of this candidate respiratory nitrate
651 reductase ($NarG_{Mn}$) is a molybdopterin oxidoreductase different from any canonical or putative
652 NarG, with no match with TIGRFAM, CDD or Pfam profiles characteristic of these proteins.
653 This $NarG_{Mn}$ does not belong to the same orthologous group alongside other typical archaeal
654 NarG (arCOG01497), but to ENOG4102T1R, which includes the well-characterised "dimethyl
655 sulfoxide reductase subunit A" (DmsA) of several *Halobacteria*. The $NarG_{Mn}$ has a high
656 similarity (>80%) with proteins from both *Methanoperedens batavicum* BLZ1 ($NarG1_{MB}$) and
657 *Methanoperedens vercellense* (Vercelli, $NarG_{MV}$) and relates to the nitrite reductases of
658 *Nitrospira defluvii* (Figure 7). While *Methanoperedens vercellense* and *M. nitroreducens* have
659 only this unusual NarG, *Methanoperedens batavicum* harbours an additional, unrelated,
660 canonical NarG ($NarG2_{MB}$) based on the detection by the TIGRFAM profile (TIGR01580,
661 arCOG01497).

662 Several of the NarG related to $NarG_{LFLS}$ (from *Halobacteria*) have been confirmed to have
663 certain promiscuity (Figure 7) and are known to be able to use (per)chlorate as a substrate *in*
664 *vivo* (Yoshimatsu et al., 2000; Oren et al., 2014). Although it is close to impossible to predict
665 the actual substrates of the $NarG_{LFLS}$ (or $PcrA_{LFLS}$), the phylogenetic analysis is, at least,
666 suggestive of the potential utilisation of (per)chlorate. The oxidation of methane linked to the
667 bioreduction of perchlorate has been proposed a number of times in the past (Luo et al., 2015;
668 Xie et al., 2018; Wu et al., 2019). Recent works (Xie et al., 2018; Wu et al., 2019) have
669 suggested the possible involvement of ANME archaea in (per)chlorate reduction based on
670 chemical and amplicon data analyses, an assumption considered more likely given that nitrate
671 was rarely measured in noticeable concentrations in the LFLS sampling trench (Vázquez-
672 Campos et al., 2017). Indeed, nitrate concentrations were below the detection limit (<0.01 μM)
673 before any *Methanoperedens* became relatively abundant. With LFLS historical disposal
674 records indicating that quantities of perchlorate/perchloric acid were deposited in the vicinity
675 of the sample location, it collectively suggests that *Methanoperedens* spp. utilisation of nitrate
676 is unlikely at the site. However, as no chlorite dismutase gene was found in any of the MAGs,
677 the possibility that they may utilise perchlorate is also not well supported. Given the high iron
678 concentrations, it is reasonable to assume that the AOM at LFLS uses Fe(III) as the main
679 electron acceptor.

680 The collective evidence indicates that nitrate reductase(-like) enzymes are rather widespread
681 in *Methanoperedens* spp., with the exception of '*Ca.* M. ferrireducens' from which no nitrate
682 reductase candidate could be detected, aside from an orphan NapA-like protein (cd02754).
683 Phylogenetic analysis of the NarG and similar proteins (Figure 7) suggests that these proteins
684 might have been horizontally acquired at least three different times during the evolution of
685 *Methanoperedens*. Congruently, the pangenomic analysis showed three different NarG variants
686 in their respective gene clusters (Figure 6 and Figure 7).

High-heme cytochromes

Analysis of historical disposal records revealed that over 760 (intact and partially corroded) steel drums were deposited within the legacy trenches at LFLS, including in close proximity of the collected samples (Payne, 2012). The unabated redox oscillations which have occurred in the trenches over the last 60+ years and the resultant impact upon the steel drums, have likely contributed to the elevated concentrations of soluble iron observed (~0.5–1 mM) (Vázquez-Campos et al., 2017).

Utilisation of metals (e.g. Fe, Mn, Cr, U) as electron acceptors requires the presence of multi-heme cytochromes. Although multi-heme cytochromes are not intrinsically and exclusively employed for heavy metal reduction (e.g. decaheme DmsE for DMSO reduction), HHC are characteristic of microorganisms performing biological reduction of metals. In our case, HHC were found in all new and reference *Methanoperedens*, including a gene cluster from the core genome. This may well indicate that oxidised metal species were the ancestral electron acceptor to all *Methanoperedens*, rather than nitrate or other non-metallic oxyanion moieties.

Previous studies indicate that *M. batavicum* and *M. ferrireducens* can both use the Fe(III) (oxyhydr)oxide ferrihydrite as electron acceptor for AOM (Ettwig et al., 2016; Cai et al., 2018). Reports showing the involvement of more crystalline forms of iron oxides for the AOM are scarce with the possibility that these organisms may drive a cryptic sulfate reduction cycle rather than a more direct Fe(III)-dependent AOM (Sivan et al., 2014). Based on the evidence to hand, it is not clear whether *Methanoperedenaceae* archaea or other ANME could be responsible for these observations.

Tantalising questions remain as to the role of *Methanoperedens* spp. with regard to the ultimate fate of iron within the legacy trenches; an important consideration given the central role that

710 iron plays in the mobilisation/retardation of key contaminants plutonium and americium
711 (Ikeda-Ohno et al., 2014; Vázquez-Campos et al., 2017).

712 PHA biosynthesis

713 Variable nutrient levels can result in the microbial production of polyhydroxyalkanoates
714 (PHA), which are carbon-rich, energetic polymers resulting from the polymerisation of
715 hydroxyalkanoates (Reddy et al., 2003; Martínez-Gutiérrez et al., 2018). The biosynthesis of
716 PHA is a widespread characteristic in many groups of aerobic *Bacteria* (Reddy et al., 2003;
717 Martínez-Gutiérrez et al., 2018). However, very few strict anaerobes are able to synthesise
718 PHA, being mostly limited to syntrophic bacteria (Spang et al., 2012). In *Archaea*, the
719 biosynthesis of PHA is known to occur, particularly in many *Nitrososphaerales*
720 (*Thaumarchaeota*) (Spang et al., 2012) and *Euryarchaeota*, where it has been traditionally
721 limited to *Halobacteria* (Koller, 2019).

722 Key genes, as well as full operons, have been detected in several *Methanoperedens* genomes,
723 with recent experimental evidence identifying the production of PHA by *Methanoperedens*
724 *nitroreducens* (Cai et al., 2019). This suggests that the biosynthesis of PHA could be a
725 widespread feature in *Methanoperedens* spp. or even in all *Methanoperedenaceae*, indicating
726 a possible, generalised, role in the accumulation of excess carbon at times when the carbon
727 source (methane) is much more abundant than other nutrients and/or trace elements
728 (Karthikeyan et al., 2015).

729 It has been estimated that anaerobic methane oxidisers may consume up to 80–90% of the
730 methane produced in certain environments, mitigating its release to the atmosphere (Reeburgh,
731 2007). The capacity of *Methanoperedens* spp. to accumulate PHA might have implications for
732 the further refinement of these estimates. The inference being that methane would not solely
733 be used for energy production or to increase cell numbers, and that *Methanoperedens* spp.

734 could act as a ‘carbon-capture’ device, especially within carbon-rich anoxic environments
735 whenever they are the main anaerobic methane oxidisers. This would likely be the case for the
736 LFLS test trench, where ammonium, nitrate/nitrite and total dissolved nitrogen are limiting.

737 Conclusion

738 While the *Archaea* inhabiting the LFLS trench water constitute a relatively small portion of its
739 microbial community, they have important roles in biogeochemical cycling, especially with
740 respect to methanogenesis, anaerobic methane oxidation and Fe(III) reduction. The diverse
741 *Methanoperedens* spp. are of special relevance due to their role in methane capture (and
742 subsequent conversion to PHA), Fe cycling, and dissimilatory pathways for nitrate and,
743 possibly, (per)chlorate reduction.

744 The broad phylogenetic representation of DPANN organisms, which have attracted particular
745 attention in recent years, either for their unusual characteristics or their controversial
746 evolutionary history, is another interesting feature of the LFLS archaeal community. The
747 description and evaluation of the MAGs from lineages LFWA-I to IV constitutes a detailed
748 first examination of several undescribed archaeal lineages.

749 The proposed LFWA-III lineages, ‘*Ca.* Gugararchaeales’ and ‘*Ca.* Anstonellales’ are amongst
750 the most interesting. Foremost, they are together unusually diverse at LFLS, with 10 out of the
751 37 MAGs recovered in this study belonging to the two orders, with two families and two genera
752 (and species) newly proposed within each order. Furthermore, they have a cohesive central
753 metabolism that likely spans the entire order with full pathways for the *de novo* biosynthesis
754 of nucleotides, most amino acids, and several vitamins/cofactors. This is duly reflected in the
755 proposed name ‘*Ca.* Gugararchaeum adminiculabundum`, proposed type for LFWA-IIIa,

where the specific epithet translates as “self-supporting” relating to the possibility of not needing a symbiotic partner.

Taxonomic Appendix

Due to several irregularities in the process of naming candidate lineages, the European Nucleotide Archive does not allow certain taxonomic names at taxonomic levels where they should exist. For example, the candidate phylum *Micrarchaeota*, and its defining candidate species '*Ca.* Micrarchaeum acidophilum', have no defined nomenclature at class, order, or family levels. This and other issues related to the nomenclature of uncultivated Bacteria and *Archaea* have been previously discussed in the literature (Whitman, 2016; Konstantinidis et al., 2017, 2019; Oren and Garrity, 2018; Chuvochina et al., 2019; Rosselló-Móra and Whitman, 2019) and we will not provide further discussion on this matter.

Nonetheless, in order to cover these gaps, we feel obliged to suggest several of these intermediate nomenclatural levels, many of which are already covered in the GTDB but not formally proposed in the literature, in addition to the nomenclatural novelties intrinsic to this manuscript.

Description of '*Candidatus* Tiddalikarchaeum' gen. nov.

'*Candidatus* Tiddalikarchaeum' (Ti.dda.lik.ar.chae'um. Gunai language, Tiddalik, frog from the Australian Aboriginal mythology; N.L. neut. n. *archaeum*, archaeon, from Gr. adj. *archaios –ê –on*, ancient; N.L. n. neut. *Tiddalikarchaeum*, the archaeon named after the greedy Aboriginal mythological Australian frog that burst with water, referring to the bathtub effect exhibited by the disposal trenches at the Little Forest Legacy Site).

The type species is '*Candidatus* Tiddalikarchaeum anstoanum'.

779 **Description of '*Candidatus* Tiddalikarchaeum anstoanum' sp. nov.**

780 '*Candidatus* Tiddalikarchaeum anstoanum' (ans.to.a'num. N.L. neut. adj. from ANSTO,
781 Australian Nuclear Science and Technology Organisation, institution managing the Little
782 Forest Legacy Site).

783 The type material is the metagenome assembled genome (MAG) LFW-252_1 (ERS2655302)
784 recovered from the groundwater of the Little Forest Legacy Site (NSW, Australia). The MAG
785 consists of 1.16 Mbp in 56 contigs with an estimated completeness of 95.7%, redundancy of
786 1.1%, 16S, 23S, and 5S rRNA gene, and 21 tRNAs. The GC content of this MAG is 36.5%.

787 **Description of '*Candidatus* Tiddalikarchaeaceae' fam. nov.**

788 *Tiddalikarchaeaceae* (Ti.dda.lik.ar.chae.a'ce.ae. N.L. neut. n. *Tiddalikarchaeum* a candidate
789 genus; -*aceae*, ending to denote a family; N.L. fem. pl. n. *Tiddalikarchaeaceae*, the
790 *Tiddalikarchaeum* candidate family).

791 The family '*Candidatus* Tiddalikarchaeaceae' is circumscribed based on two independent
792 concatenated protein phylogenies of 44 and 91 markers, the latter also supported by the rank
793 normalisation approach as per Parks et al. (2018). The description is the same as that of its sole
794 genus and species. The type genus is '*Candidatus* Tiddalikarchaeum'.

795 **Description of '*Candidatus* Tiddalikarchaeales' ord. nov.**

796 '*Candidatus* Tiddalikarchaeales' (Ti.dda.lik.ar.chae.a'les. N.L. neut. n. *Tiddalikarchaeum* a
797 candidate genus; -*ales*, ending to denote an order; N.L. fem. pl. n. *Tiddalikarchaeales* the
798 *Tiddalikarchaeum* candidate order).

799 The order '*Candidatus* Tiddalikarchaeales' is circumscribed based on two independent
800 concatenated protein phylogenies of 44 and 91 markers, the latter also supported by the rank

801 normalisation approach as per Parks et al. (2018). The description is the same as that of its sole
802 genus and species. The type genus is '*Candidatus* Tiddalikarchaeum'.

803 The order is equivalent to CG07-land from Probst, et al. (2018) or o__CG07-land in GTDB
804 r89 (Parks et al., 2017).

805 **Description of "*Nanoarchaeia*" class. nov.**

806 "*Nanoarchaeia*" (Na.no.ar.chae'ia. N.L. neut. n. "*Nanoarchaeum*", a genus; -*ia*, ending to
807 denote a class; N.L. fem. pl. n. "*Nanoarchaeia*", the "*Nanoarchaeum*" candidate class).

808 The class "*Nanoarchaeia*" is circumscribed based on two independent concatenated protein
809 phylogenies of 44 and 91 markers, the latter also supported by the rank normalisation approach
810 as per Parks et al. (2018). The description is the same as that of its sole genus and species. The
811 class "*Nanoarchaeia*" is defined as the most inclusive class that includes the genus
812 "*Nanoarchaeum*". The lineages *Parvarchaeota* (Rinke et al., 2013), *Woesearchaeota* and
813 *Pacearchaeota* (Castelle et al., 2015), and order '*Candidatus* Tiddalikarchaeales' (this work)
814 are contained within "*Nanoarchaeia*". The type order is "*Nanoarchaeales*" Huber, Auerbach
815 and Podar (2016).

816 This class is the only class within "*Nanoarchaeota*" Huber & Kreuter (2014), and equivalent
817 to the c__Nanoarchaeia in the GTDB r89 (Parks et al., 2017).

818 **Description of '*Candidatus* Gugararchaeum' gen. nov.**

819 '*Candidatus* Gugararchaeum' (Gu.ga.rar.chae'um. Dharawal language, *gugara*, kookaburra –
820 bird endemic to Australia, *Dacelo* spp.; N.L. neut. n. *archaeum*, archaeon, from Gr. adj.
821 *archaios –ê –on*, ancient; N.L. neut. n. *Gugararchaeum*, the kookaburra archaeon, honouring
822 the bird, common at the Little Forest Legacy Site, bird emblem of NSW, and typical across
823 Australia).

824 The type species is '*Candidatus* Gugararchaeum adminiculabundum'.

825 **Description of '*Candidatus* Gugararchaeum adminiculabundum' sp. nov.**

826 '*Candidatus* Gugararchaeum adminiculabundum' (ad.mi.ni.cu.la.bun'dum. L. adj. neut. self-
827 supporting; in reference to the limited external requirements and its suggested independence
828 from a host/symbiote, due to the predicted presence of pathways for the biosynthesis of amino
829 acids, purines, pyrimidines, thiamine, and riboflavin).

830 The type material is the metagenome assembled genome (MAG) LFW-121_3 (ERS2655302)
831 recovered from the groundwater of the Little Forest Legacy Site (NSW, Australia). The MAG
832 consists of 1.47 Mbp in 76 contigs with an estimated completeness of 96.8%, redundancy of
833 2.2%, 16S, 23S, and 5S rRNA gene, and 21 tRNAs. The GC content of this MAG is 49.8%.

834 **Description of '*Candidatus* Gugararchaeaceae' fam. nov.**

835 '*Candidatus* Gugararchaeaceae' (Gu.ga.rar.chae.a'ce.ae. N.L. neut. n. *Gugararchaeum*, a
836 candidate genus; -*aceae*, ending to denote a family. N.L. fem. pl. n. *Gugararchaeaceae*, the
837 *Gugararchaeum* candidate family).

838 The family '*Candidatus* Gugararchaeaceae' is circumscribed based on two independent
839 concatenated protein phylogenies of 44 and 91 markers, the latter also supported by the rank
840 normalisation approach as per Parks et al. (2018). The description is the same as that of its sole
841 genus and species. The type genus is '*Candidatus* Gugararchaeum'.

842 **Description of '*Candidatus* Burarchaeum' gen. nov.**

843 '*Candidatus* Burarchaeum' (Bu.rar.chae'um. Dharawal language, *buru*, kangaroo; N.L. neut.
844 n. *archaeum*, archaeon, from Gr. adj. *archaios –ê –on*, ancient; N. L. neut. n. *Burarchaeum*, an
845 archaeon from the land of the kangaroos, also faunal emblem of Australia).

846 The type species is '*Candidatus* Burarchaeum australiense'.

847 **Description of '*Candidatus* Burarchaeum australiense' sp. nov.**

848 '*Candidatus* Burarchaeum australiense' (aus.tra.lien'se. N.L. neut. adj. referring to Australia,
849 country where its first genome was reconstructed).

850 The type material is the metagenome assembled genome (MAG) LFW-281_7 (ERS2655318)
851 recovered from the groundwater of the Little Forest Legacy Site (NSW, Australia). The MAG
852 consists of 1.20 Mbp in 76 contigs with an estimated completeness of 96.8%, redundancy of
853 5.4%, 16S and 5S rRNA gene, and 18 tRNAs. The GC content of this MAG is 57.6%.

854 **Description of '*Candidatus* Burarchaeaceae' fam. nov.**

855 '*Candidatus* Burarchaeaceae' (Bu.rar.chae.a'ce.ae. N.L. neut. n. *Burarchaeum*, a candidate
856 genus; -*aceae*, ending to denote a family. N.L. fem. pl. n. *Burarchaeaceae*, the *Burarchaeum*
857 candidate family).

858 The family '*Candidatus* Burarchaeaceae' is circumscribed based on two independent
859 concatenated protein phylogenies of 44 and 91 markers, the latter also supported by the rank
860 normalisation approach as per Parks et al. (2018). The description is the same as that of its sole
861 genus and species. The type genus is '*Candidatus* Burarchaeum'.

862 **Description of '*Candidatus* Gugararchaeales' ord. nov.**

863 '*Candidatus* Gugararchaeales' (Gu.ga.rar.chae.a'les. N.L. neut. n. *Gugararchaeum*, a
864 candidate genus; -*ales*, ending to denote an order; N.L. fem. pl. n. *Gugararchaeales*, the
865 *Gugararchaeum* candidate order).

866 The order '*Candidatus* Gugararchaeales' is circumscribed based on two independent
867 concatenated protein phylogenies of 44 and 91 markers, the latter also supported by the rank

868 normalisation approach as per Parks et al. (2018). It constitutes the most inclusive clade that
869 includes the families '*Candidatus* Gugararchaeaceae', and '*Candidatus* Burarchaeaceae'. The
870 type genus is '*Candidatus* Gugararchaeum'.

871 The order is equivalent to LFWA-IIIa in this manuscript, and o__UBA10214 in the GTDB r89
872 (Parks et al., 2017).

873 **Description of '*Candidatus* Anstonella' gen. nov.**

874 '*Candidatus* Anstonella' (Ans.to.ne'lla. N.L. dim. n. fem. *Anstonella* from ANSTO, Australian
875 Nuclear Science and Technology Organisation, institution managing the Little Forest Legacy
876 Site).

877 The type species is '*Candidatus* Anstonella stagnisolia'

878 **Description of '*Candidatus* Anstonella stagnisolia' sp. nov.**

879 '*Candidatus* Anstonella stagnisolia' (s.tag.ni.so'lia. L. v. *stagno* overflow; L. neut. n. *solium* -
880 *a* tub, bathtub; N.L. adj. fem. *stagnisolia*, overflowing bathtub, in reference to the phenomenon
881 described during heavy rainfalls at the Little Forest Legacy Site trenches).

882 The type material is the metagenome assembled genome (MAG) LFW-35 (ERS2655287)
883 recovered from the groundwater of the Little Forest Legacy Site (NSW, Australia). The MAG
884 consists of 1.33 Mbp in 68 contigs with an estimated completeness of 97.8%, redundancy of
885 2.2%, 16S, 23S and 5S rRNA gene, and 21 tRNAs. The GC content of this MAG is 50.3%.

886 **Description of '*Candidatus* Anstonellaceae' fam. nov.**

887 '*Candidatus* Anstonellaceae' (Ans.to.nel.la'ce.ae. N.L. neut. n. *Anstonella*, a candidate genus;
888 -*aceae*, ending to denote a family; N.L. fem. pl. n. *Anstonellaceae*, the *Anstonella* candidate
889 family).

890 The family '*Candidatus* Anstonellaceae' is circumscribed based on two independent
891 concatenated protein phylogenies of 44 and 91 markers, the latter also supported by the rank
892 normalisation approach as per Parks et al. (2018). The description is the same as that of its sole
893 genus and species. The type genus is '*Candidatus* Anstonella'.

894 This family is equivalent to f__UBA10161 in the GTDB r89 (Parks et al., 2017).

895 **Description of '*Candidatus* Bilamarchaeum' gen. nov.**

896 '*Candidatus* Bilamarchaeum' (Bi.la.mar.chae'um. Dharawal language, *bilama*, freshwater
897 turtle, in reference to their presence still nowadays in the creeks and rivers associated with the
898 Little Forest Legacy Site; N.L. neut. n. *archaeum*, archaeon, from Gr. adj. *archaios –ê –on*,
899 ancient; N.L. neut. n. *Bilamarchaeum*, an archaeon from the turtle lands).

900 The type species is '*Candidatus* Bilamarchaeum dharawalense'.

901 **Description of '*Candidatus* Bilamarchaeum dharawalense' sp. nov.**

902 '*Candidatus* Bilamarchaeum dharawalense' (dha.ra.wa.len'se. N.L. neut. adj. pertaining to the
903 Dharawal, traditional owners of the lands where the Little Forest Legacy Site is located).

904 The type material is the metagenome assembled genome (MAG) LFW-283_2 (ERS2655319)
905 recovered from the groundwater of the Little Forest Legacy Site (NSW, Australia). The MAG
906 consists of 1.27 Mbp in 63 contigs with an estimated completeness of 95.7%, redundancy of
907 0%, 16S, 23S and 5S rRNA gene, and 20 tRNAs. The GC content of this MAG is 40.0%.

908 **Description of '*Candidatus* Bilamarchaeaceae' fam. nov.**

909 '*Candidatus* Bilamarchaeaceae' (Bi.la.mar.chae.a'ce.ae. N.L. neut. n. *Bilamarchaeum*, a
910 candidate genus; -*aceae*, ending to denote a family; N.L. fem. pl. n. *Bilamarchaeaceae*, the
911 *Bilamarchaeum* candidate family).

912 The family '*Candidatus* Bilamarchaeaceae' is circumscribed based on two independent
913 concatenated protein phylogenies of 44 and 91 markers, the latter also supported by the rank
914 normalisation approach as per Parks et al. (2018). The description is the same as that of its sole
915 genus and species. The type genus is '*Candidatus* Bilamarchaeum'.

916 This family is equivalent to f__UBA10214 in the GTDB r89 (Parks et al., 2017).

917 **Description of '*Candidatus* Anstonellales' ord. nov.**

918 '*Candidatus* Anstonellales' (Ans.to.nel.la'les. N.L. neut. n. *Anstonella*, a candidate genus; -
919 *ales*, ending to denote an order; N.L. fem. pl. n. *Anstonellales*, the *Anstonella* candidate order).

920 The order '*Candidatus* Anstonellales' is circumscribed based on two independent concatenated
921 protein phylogenies of 44 and 91 markers, the latter also supported by the rank normalisation
922 approach as per Parks et al. (2018). It constitutes the most inclusive clade that includes the
923 families '*Candidatus* Anstonellaceae, and '*Candidatus* Bilamarchaeaceae'. The type genus is
924 '*Candidatus* Anstonella'.

925 The order is equivalent to the lineage LFWA-IIIb in this manuscript, and o__UBA10214 in the
926 GTDB r89 (Parks et al., 2017).

927 **Description of '*Candidatus* Micrarchaeaceae' fam. nov.**

928 '*Candidatus* Micrarchaeaceae' (Mi.crar.chae'a.ce.ae. N.L. neut. n. *Micrarchaeum*, a candidate
929 genus; -*aceae*, ending to denote a family; N.L. fem. pl. n. *Micrarchaeaceae*, the *Micrarchaeum*
930 candidate family).

931 The family '*Candidatus* Micrarchaeaceae' is circumscribed based on two independent
932 concatenated protein phylogenies of 44 and 91 markers, the latter also supported by the rank
933 normalisation approach as per Parks et al. (2018). It is the most inclusive family that includes

934 the genera '*Candidatus* Micrarchaeum' and '*Candidatus* Mancarchaeum'. The type genus is
935 '*Candidatus* Micrarchaeum'.

936 **Description of '*Candidatus* Micrarchaeales' ord. nov.**

937 '*Candidatus* Micrarchaeales' (Mi.crar.chae.a'les. N.L. neut. n. *Micrarchaeum*, a candidate
938 genus; -*ales*, ending to denote an order; N.L. fem. pl. n. *Micrarchaeales*, the *Micrarchaeum*
939 candidate order).

940 The order '*Candidatus* Micrarchaeales' is circumscribed based on two independent
941 concatenated protein phylogenies of 44 and 91 markers, the latter also supported by the rank
942 normalisation approach as per Parks et al. (2018). The type genus is '*Candidatus*
943 Micrarchaeum'.

944 The order is equivalent to o__Micrarchaeales in the GTDB r89 (Parks et al., 2017).

945 **Description of '*Candidatus* Norongarragalina' gen. nov.**

946 '*Candidatus* Norongarragalina' (No.ron.ga.rra.ga.li'na. Dharawal language *Norongarragal*,
947 Dharawal clan group who traditionally occupied the Menai/Lucas Heights area where the
948 present study took place; L. fem. suff., -*ina*, pertaining or belonging to; N.L. dim. n. fem.
949 *Norongarragalina*, the archaeon from the Norongarragal clan).

950 The type species is '*Candidatus* Norongarragalina meridionalis'.

951 **Description of '*Candidatus* Norongarragalina meridionalis' sp. nov.**

952 '*Candidatus* Norongarragalina meridionalis' (me.ri.dio.na'lis. L. fem. adj. *meridionalis*,
953 southern; referring to the Southern hemisphere, where its first genome was reconstructed).

954 The type material is the metagenome assembled genome (MAG) LFW-144_1 (ERS2655293)
955 recovered from the groundwater of the Little Forest Legacy Site (NSW, Australia). The MAG

consists of 0.93 Mbp in 49 contigs with an estimated completeness of 93.5%, redundancy of 1.1%, 16S and 5S rRNA gene, and 20 tRNAs. The GC content of this MAG is 57.5%.

Description of '*Candidatus* Norongarragalinaceae' fam. nov.

'*Candidatus* Norongarragalinaceae' (No.ron.ga.rra.ga.li.na'ce.ae. N.L. neut. n. *Norongarragalina*, a candidate genus; -*aceae*, ending to denote a family; N.L. fem. pl. n. *Norongarragalinaceae*, the *Norongarragalina* candidate family).

The family '*Candidatus* Norongarragalinaceae' is circumscribed based on two independent concatenated protein phylogenies of 44 and 91 markers, the latter also supported by the rank normalisation approach as per Parks et al. (2018). The description is the same as that of its sole genus and species. The type genus is '*Candidatus* Norongarragalina'.

This family is equivalent to f__0-14-0-20-59-11 in the GTDB r89 (Parks et al., 2017).

Description of '*Candidatus* Norongarragalinales' ord. nov.

'*Candidatus* Norongarragalinales' (No.ron.ga.rra.ga.li.na'les. N.L. neut. n. *Norongarragalina*, a candidate genus; -*ales*, ending to denote an order, N.L. fem. pl. n. *Norongarragalinales*, the *Norongarragalina* candidate order).

The order '*Candidatus* Norongarragalinales' is circumscribed based on two independent concatenated protein phylogenies of 44 and 91 markers, the latter also supported by the rank normalisation approach as per Parks et al. (2018). The description is the same as that of its sole genus and species. The type genus is '*Candidatus* Norongarragalina'.

This order is equivalent to LFWA-II in this manuscript, and o__UBA8480 in GTDB r89 (Parks et al., 2017).

977 **Description of '*Candidatus* Micrarchaeia' class. nov.**

978 *Micrarchaeia* (Mi.crar.chae'ia. N.L. neut. n. *Micrarchaeum*, a candidate genus; -*ia*, ending to
979 denote a class; N.L. fem. pl. n. *Micrarchaeia*, the *Micrarchaeum* candidate class.

980 The class '*Candidatus* Micrarchaeia' is circumscribed based on two independent concatenated
981 protein phylogenies of 44 and 91 markers, the latter also supported by the rank normalisation
982 approach as per Parks et al. (2018). This class is defined as the most inclusive class that includes
983 the orders '*Candidatus* Micrarchaeales', '*Candidatus* Gugararchaeales', '*Candidatus*
984 Anstonellales', and '*Candidatus* Norongarragalinales'. The type order is '*Candidatus*
985 Micrarchaeales'.

986 This class constitutes the only class within the phylum '*Candidatus* Micrarchaeota' Baker &
987 Dick (2013). It is equivalent to the c__Micrarchaeia in the GTDB r89 (Parks et al., 2017).

988 **Description of '*Candidatus* Methanoperedens vercellense' sp. nov.**

989 '*Candidatus* Methanoperedens vercellense' (ver.cel.len'se. L. adj. pertaining or relative to
990 *Vercellae*, Latin name of Vercelli (Italy); in relation to the original MAG code designation,
991 '*Ca.* Methanoperedens nitroreducens' Vercelli, and original location of the sampling from
992 where it was retrieved).

993 The type material is the metagenome assembled genome (MAG) GCA_900196725
994 (ERS1800110) recovered from an enrichment culture for anaerobic methanotrophs derived
995 from samples collected from paddy field soil (Vercelli, Italy). The MAG consists of 3.52 Mbp
996 in 250 contigs with an estimated completeness of 96.7%, redundancy of 6.5%, 16S, 23S and
997 5S rRNA gene, and 21 tRNAs. The GC content of this MAG is 44.1%. Differentiated from
998 other '*Ca.* Methanoperedens spp.' based on ANI and AAI.

999 **Description of '*Candidatus* Methanoperedens batavicum' sp. nov.**

1000 '*Candidatus* Methanoperedens batavicum' (ba'ta.vi.cum L. adj. *batavicum -us*, relative or
1001 pertaining to Batavia (*Ulpia Noviomagus Batavorum*), Latin name of Nijmegen, in reference
1002 to the Radboud University Nijmegen, where the initial genome, '*Ca.* Methanoperedens
1003 nitroreducens' BLZ1, was studied).

1004 The type material is the metagenome assembled genome (MAG) BLZ1
1005 (GCA_001317315/LKCM00000000.1) recovered from a bioreactor for the enrichment of
1006 anaerobic methanotrophs at the Radboud University Nijmegen (Nijmegen, The Netherlands).
1007 The MAG consists of 3.74 Mbp in 514 contigs with an estimated completeness of 95.8%,
1008 redundancy of 6.6%, 16S, 23S and 5S rRNA gene, and 21 tRNAs. The GC content of this MAG
1009 is 40.8%. Differentiated from other '*Ca.* Methanoperedens spp.' based on ANI and AAI.

Acknowledgements

We acknowledge Shane Ingrey and Raymond Ingrey from the Dharawal Language Program from the Gujaga Fundation for their assistance with the Dharawal language and with their views on aboriginal matters in general. MRW acknowledges the support of the Australian Federal Government NCRIS scheme, via Bioplatforms Australia. MRW and XVC acknowledge support from the New South Wales State Government RAAP scheme and the UNSW RIS scheme. ASK, TEP and TDW acknowledge funding by the Australian Research Council (Discovery Project DP210103727) as well as from the Australian Nuclear Science and Technology Organisation (ANSTO).

Conflict of Interest

The authors declare that they have no conflict of interest.

Contribution statement

XVC: Conceptualization, Data curation, Formal analysis, Investigation, Methodology, Project administration, Visualization, Writing – original draft, Writing – review & editing. ASK: Writing – original draft, Writing – review & editing. MWB: Writing – review & editing. MRW: Resources, Supervision, Writing – review & editing. TEP: Resources, Site-specific expertise, Funding acquisition, Project administration. TDW: Resources, Funding acquisition, Project administration, Supervision, Writing – review & editing.

References

Adam, P. S., Borrel, G., Brochier-Armanet, C., and Gribaldo, S. (2017). The growing tree of Archaea: new perspectives on their diversity, evolution and ecology. *ISME J.* doi:10/gbrbh4.

Akiva, E., Brown, S., Almonacid, D. E., Barber, A. E., Custer, A. F., Hicks, M. A., et al. (2014). The Structure–Function Linkage Database. *Nucleic Acids Res* 42, D521–D530. doi:10/gf5cgq.

Alneberg, J., Bjarnason, B. S., de Bruijn, I., Schirmer, M., Quick, J., Ijaz, U. Z., et al. (2014). Binning metagenomic contigs by coverage and composition. *Nat Meth* 11, 1144–1146. doi:10/f25cs2.

Anantharaman, K., Brown, C. T., Hug, L. A., Sharon, I., Castelle, C. J., Probst, A. J., et al. (2016). Thousands of microbial genomes shed light on interconnected biogeochemical processes in an aquifer system. *Nat Commun* 7, 13219. doi:10/f88b9n.

André, I., Potocki-Véronèse, G., Barbe, S., Moulis, C., and Remaud-Siméon, M. (2014). CAZyme discovery and design for sweet dreams. *Curr Opin Chem Biol* 19, 17–24. doi:10/f547c5.

Aramaki, T., Blanc-Mathieu, R., Endo, H., Ohkubo, K., Kanehisa, M., Goto, S., et al. (2020). KofamKOALA: KEGG Ortholog assignment based on profile HMM and adaptive score threshold. *Bioinformatics* 36, 2251–2252. doi:10/ghk6qt.

Arshad, A., Speth, D. R., de Graaf, R. M., Op den Camp, H. J. M., Jetten, M. S. M., and Welte, C. U. (2015). A metagenomics-based metabolic model of nitrate-dependent anaerobic oxidation of methane by *Methanoperedens*-like Archaea. *Front Microbiol* 6, 1423. doi:10/gccwvw.

Attwood, T. K., Beck, M. E., Bleasby, A. J., and Parry-Smith, D. J. (1994). PRINTS--a database of protein motif fingerprints. *Nucleic Acids Res* 22, 3590–3596.

Baker, B. J., and Dick, G. J. (2013). Omic Approaches in Microbial Ecology: Charting the Unknown: Analysis of whole-community sequence data is unveiling the diversity and function of specific microbial groups within uncultured phyla and across entire microbial ecosystems. *Microbe* 8, 353–360. doi:10/gj6qsg.

Baker, B. J., Tyson, G. W., Webb, R. I., Flanagan, J., Hugenholtz, P., Allen, E. E., et al. (2006). Lineages of acidophilic Archaea revealed by community genomic analysis. *Science* 314, 1933–1935. doi:10/c7k3kh.

Buelow, H. N., Winter, A. S., Van Horn, D. J., Barrett, J. E., Gooseff, M. N., Schwartz, E., et al. (2016). Microbial Community Responses to Increased Water and Organic Matter in the Arid Soils of the McMurdo Dry Valleys, Antarctica. *Front Microbiol* 7. doi:10/gjs49h.

1064 Cai, C., Leu, A. O., Xie, G.-J., Guo, J., Feng, Y., Zhao, J.-X., et al. (2018). A methanotrophic
1065 archaeon couples anaerobic oxidation of methane to Fe(III) reduction. *ISME J* 12,
1066 1929–1939. doi:10/gc95d7.

1067 Cai, C., Shi, Y., Guo, J., Tyson, G. W., Hu, S., and Yuan, Z. (2019). Acetate production from
1068 anaerobic oxidation of methane via intracellular storage compounds. *Environ Sci*
1069 *Technol*, Just accepted. doi:10/gf3svt.

1070 Castelle, C. J., Wrighton, K. C., Thomas, B. C., Hug, L. A., Brown, C. T., Wilkins, M. J., et al.
1071 (2015). Genomic expansion of domain archaea highlights roles for organisms from new
1072 phyla in anaerobic carbon cycling. *Curr Biol* 25, 690–701. doi:10/f65pk9.

1073 Chan, P. P., Lin, B. Y., Mak, A. J., and Lowe, T. M. (2019). tRNAscan-SE 2.0: Improved
1074 Detection and Functional Classification of Transfer RNA Genes. *bioRxiv*, 614032.
1075 doi:10/gf3xsp.

1076 Chaumeil, P.-A., Mussig, A. J., Hugenholtz, P., and Parks, D. H. (2020). GTDB-Tk: a toolkit
1077 to classify genomes with the Genome Taxonomy Database. *Bioinformatics* 36, 1925–
1078 1927. doi:10/ggc9dd.

1079 Chen, L.-X., Méndez-García, C., Dombrowski, N., Servín-Garcidueñas, L. E., Eloe-Fadrosh,
1080 E. A., Fang, B.-Z., et al. (2018). Metabolic versatility of small archaea Micrarchaeota
1081 and Parvarchaeota. *ISME J* 12, 756–775. doi:10/gc8qh2.

1082 Chuvochina, M., Rinke, C., Parks, D. H., Rappé, M. S., Tyson, G. W., Yilmaz, P., et al. (2019).
1083 The importance of designating type material for uncultured taxa. *Syst Appl Microbiol*
1084 42, 15–21. doi:10/gdtnf4.

1085 Criscuolo, A., and Gribaldo, S. (2010). BMGE (Block Mapping and Gathering with Entropy):
1086 a new software for selection of phylogenetic informative regions from multiple
1087 sequence alignments. *BMC Evolutionary Biology* 10, 210. doi:10/dh3zsr.

1088 Darling, A. E., Jospin, G., Lowe, E., Iv, F. A. M., Bik, H. M., and Eisen, J. A. (2014). PhyloSift:
1089 phylogenetic analysis of genomes and metagenomes. *PeerJ* 2, e243. doi:10/gddvvt.

1090 Dombrowski, N., Lee, J.-H., Williams, T. A., Offre, P., and Spang, A. (2019). Genomic
1091 diversity, lifestyles and evolutionary origins of DPANN archaea. *FEMS Microbiol Lett*
1092 366, fnz008. doi:10/gftfpk.

1093 Dombrowski, N., Seitz, K. W., Teske, A. P., and Baker, B. J. (2017). Genomic insights into
1094 potential interdependencies in microbial hydrocarbon and nutrient cycling in
1095 hydrothermal sediments. *Microbiome* 5, 106. doi:10/gbt9qt.

1096 Dombrowski, N., Williams, T. A., Sun, J., Woodcroft, B. J., Lee, J.-H., Minh, B. Q., et al.
1097 (2020). Undinarchaeota illuminate DPANN phylogeny and the impact of gene transfer
1098 on archaeal evolution. *Nat Commun* 11, 3939. doi:10/gjfkfr.

1099 Eddy, S. R. (2011). Accelerated profile HMM searches. *PLoS Comput Biol* 7, e1002195.
1100 doi:10/dx4kqk.

1101 Eren, A. M., Esen, Ö. C., Quince, C., Vineis, J. H., Morrison, H. G., Sogin, M. L., et al. (2015).
1102 Anvi'o: an advanced analysis and visualization platform for 'omics data. *PeerJ* 3,
1103 e1319. doi:10/gftphk.

1104 Eren, A. M., Kiefl, E., Shaiber, A., Veseli, I., Miller, S. E., Schechter, M. S., et al. (2021).
1105 Community-led, integrated, reproducible multi-omics with anvi'o. *Nat Microbiol* 6, 3–
1106 6. doi:10/ghqc54.

1107 Ettwig, K. F., Zhu, B., Speth, D., Keltjens, J. T., Jetten, M. S. M., and Kartal, B. (2016).
1108 Archaea catalyze iron-dependent anaerobic oxidation of methane. *PNAS* 113, 12792–
1109 12796. doi:10/f9cvgs.

1110 Finn, R. D., Bateman, A., Clements, J., Coggill, P., Eberhardt, R. Y., Eddy, S. R., et al. (2014).
1111 Pfam: the protein families database. *Nucleic Acids Res* 42, D222–D230. doi:10/f25qtg.

1112 Golyshina, O. V., Toshchakov, S. V., Makarova, K. S., Gavrilov, S. N., Korzhenkov, A. A.,
1113 Cono, V. L., et al. (2017). 'ARMAN' archaea depend on association with euryarchaeal
1114 host in culture and in situ. *Nat Commun* 8, 60. doi:10/gfb5tb.

1115 Gough, J., Karplus, K., Hughey, R., and Chothia, C. (2001). Assignment of homology to
1116 genome sequences using a library of hidden Markov models that represent all proteins
1117 of known structure. *J Mol Biol* 313, 903–919. doi:10/bqw5vg.

1118 Grosjean, H., and Westhof, E. (2016). An integrated, structure- and energy-based view of the
1119 genetic code. *Nucleic Acids Res* 44, 8020–8040. doi:10/f9fjkd.

1120 Haft, D. H., Selengut, J. D., Richter, R. A., Harkins, D., Basu, M. K., and Beck, E. (2013).
1121 TIGRFAMs and Genome Properties in 2013. *Nucleic Acids Res* 41, D387–D395.
1122 doi:10/ggbwr6.

1123 Haroon, M. F., Hu, S., Shi, Y., Imelfort, M., Keller, J., Hugenholtz, P., et al. (2013). Anaerobic
1124 oxidation of methane coupled to nitrate reduction in a novel archaeal lineage. *Nature*
1125 500, 567–570. doi:10/f48h4q.

1126 He, L., Zhong, Y., Yao, F., Chen, F., Xie, T., Wu, B., et al. (2019). Biological perchlorate
1127 reduction: which electron donor we can choose? *Environ Sci Pollut Res* 26, 16906–
1128 16922. doi:10/ggb5xj.

1129 Hoang, D. T., Chernomor, O., von Haeseler, A., Minh, B. Q., and Vinh, L. S. (2018). UFBoot2:
1130 Improving the Ultrafast Bootstrap Approximation. *Mol Biol Evol* 35, 518–522.
1131 doi:10/gcxrqg.

1132 Huber, H., Auerbach, A., and Podar, M. (2016). "'Nanoarchaeales,'" in *Bergey's Manual of*
1133 *Systematics of Archaea and Bacteria* (American Cancer Society), 1–2.
1134 doi:10.1002/9781118960608.obm00129.

1135 Huber, H., Hohn, M. J., Rachel, R., Fuchs, T., Wimmer, V. C., and Stetter, K. O. (2002). A
1136 new phylum of Archaea represented by a nanosized hyperthermophilic symbiont.
1137 *Nature* 417, 63–67. doi:10/drfqds.

1138 Huber, H., and Kreuter, L. (2014). "The Phylum Nanoarchaeota," in *The Prokaryotes: Other*
1139 *Major Lineages of Bacteria and The Archaea*, eds. E. Rosenberg, E. F. DeLong, S.

Lory, E. Stackebrandt, and F. Thompson (Berlin, Heidelberg: Springer), 311–318. doi:10.1007/978-3-642-38954-2_337.

Huerta-Cepas, J., Forslund, K., Coelho, L. P., Szklarczyk, D., Jensen, L. J., von Mering, C., et al. (2017). Fast genome-wide functional annotation through orthology assignment by eggNOG-mapper. *Mol Biol Evol* 34, 2115–2122. doi:10/ggbwwj.

Huerta-Cepas, J., Szklarczyk, D., Forslund, K., Cook, H., Heller, D., Walter, M. C., et al. (2016). eggNOG 4.5: a hierarchical orthology framework with improved functional annotations for eukaryotic, prokaryotic and viral sequences. *Nucleic Acids Res* 44, D286–D293. doi:10/f8cmvq.

Hug, L. A., Baker, B. J., Anantharaman, K., Brown, C. T., Probst, A. J., Castelle, C. J., et al. (2016). A new view of the tree of life. *Nat Microbiol*, 16048. doi:10/bpkh.

Ikeda-Ohno, A., Harrison, J. J., Thiruvoth, S., Wilsher, K., Wong, H. K. Y., Johansen, M. P., et al. (2014). Solution speciation of plutonium and americium at an Australian legacy radioactive waste disposal site. *Environ Sci Technol* 48, 10045–10053. doi:10/ggbwp6.

John, S. G., Mendez, C. B., Deng, L., Poulos, B., Kauffman, A. K. M., Kern, S., et al. (2011). A simple and efficient method for concentration of ocean viruses by chemical flocculation. *Environ Microbiol Rep* 3, 195–202. doi:10/brktnw.

Jones, P., Binns, D., Chang, H.-Y., Fraser, M., Li, W., McAnulla, C., et al. (2014). InterProScan 5: genome-scale protein function classification. *Bioinformatics* 30, 1236–1240. doi:10/f53532.

Kanehisa, M., Sato, Y., Kawashima, M., Furumichi, M., and Tanabe, M. (2016). KEGG as a reference resource for gene and protein annotation. *Nucleic Acids Res* 44, D457–D462. doi:10/f8cqdp.

Karp, P. D., Latendresse, M., Paley, S. M., Krummenacker, M., Ong, Q. D., Billington, R., et al. (2016). Pathway Tools version 19.0 update: software for pathway/genome informatics and systems biology. *Brief Bioinform* 17, 877–890. doi:10/f89mmb.

Karthikeyan, O. P., Chidambarampadmavathy, K., Cirés, S., and Heimann, K. (2015). Review of sustainable methane mitigation and biopolymer production. *Crit Rev Environ Sci Technol* 45, 1579–1610. doi:10/gfvpz6.

Kinsela, A. S., Bligh, M., Vázquez-Campos, X., Sun, Y., Wilkins, M. R., Comarmond, M. J., et al. (2021). Biogeochemical Mobility of Contaminants from a Replica Radioactive Waste Trench in Response to Rainfall-induced Redox Oscillations. *Environ Sci Technol*. doi:10/gkhz9g.

Kitzinger, K., Padilla, C. C., Marchant, H. K., Hach, P. F., Herbold, C. W., Kidane, A. T., et al. (2019). Cyanate and urea are substrates for nitrification by Thaumarchaeota in the marine environment. *Nat Microbiol* 4, 234. doi:10/gfpkzg.

Knittel, K., and Boetius, A. (2009). Anaerobic oxidation of methane: progress with an unknown process. *Annu Rev Microbiol* 63, 311–334. doi:10/bsbxwq.

1178 Koller, M. (2019). Polyhydroxyalkanoate biosynthesis at the edge of water activity-
1179 Haloarchaea as biopolyester factories. *Bioengineering* 6, 34. doi:10/gf4bcr.

1180 Konstantinidis, K. T., Rosselló-Móra, R., and Amann, R. (2017). Uncultivated microbes in
1181 need of their own taxonomy. *ISME J* 11, 2399–2406. doi:10/gbprgw.

1182 Konstantinidis, K. T., Rossello-Mora, R., and Amann, R. (2019). Moving the cataloguing of
1183 the "uncultivated majority" forward. *Syst Appl Microbiol* 42, 3–4. doi:10/gfv22j.

1184 Lazar, C. S., Baker, B. J., Seitz, K. W., and Teske, A. P. (2017). Genomic reconstruction of
1185 multiple lineages of uncultured benthic archaea suggests distinct biogeochemical roles
1186 and ecological niches. *ISME J* 11, 1118–1129. doi:10/f9mkgc.

1187 Le, S. Q., Gascuel, O., and Lartillot, N. (2008). Empirical profile mixture models for
1188 phylogenetic reconstruction. *Bioinformatics* 24, 2317–2323. doi:10/fj3qpw.

1189 Lee, M. D. (2019). GToTree: a user-friendly workflow for phylogenomics. *Bioinformatics* 35,
1190 4162–4164. doi:10/gfxbbx.

1191 Lees, J. G., Lee, D., Studer, R. A., Dawson, N. L., Sillitoe, I., Das, S., et al. (2014). Gene3D:
1192 Multi-domain annotations for protein sequence and comparative genome analysis.
1193 *Nucleic Acids Res* 42, D240–D245. doi:10/f5sh7d.

1194 Letunic, I., Doerks, T., and Bork, P. (2015). SMART: recent updates, new developments and
1195 status in 2015. *Nucleic Acids Res* 43, D257–D260. doi:10/f64qr5.

1196 Li, D., Liu, C.-M., Luo, R., Sadakane, K., and Lam, T.-W. (2015). MEGAHIT: an ultra-fast
1197 single-node solution for large and complex metagenomics assembly via succinct de
1198 Bruijn graph. *Bioinformatics* 31, 1674–1676. doi:10/f7fb5z.

1199 Li, D., Luo, R., Liu, C.-M., Leung, C.-M., Ting, H.-F., Sadakane, K., et al. (2016). MEGAHIT
1200 v1.0: a fast and scalable metagenome assembler driven by advanced methodologies and
1201 community practices. *Methods* 102, 3–11. doi:10/f8q7mg.

1202 Li, W., and Godzik, A. (2006). Cd-hit: a fast program for clustering and comparing large sets
1203 of protein or nucleotide sequences. *Bioinformatics* 22, 1658–1659. doi:10/ct8g72.

1204 Lledó, B., Martínez-Espinosa, R. M., Marhuenda-Egea, F. C., and Bonete, M. J. (2004).
1205 Respiratory nitrate reductase from haloarchaeon *Haloferax mediterranei*: biochemical
1206 and genetic analysis. *Biochim Biophys Acta Gen Subj* 1674, 50–59. doi:10/b78br8.

1207 Lu, Y.-Z., Fu, L., Ding, J., Ding, Z.-W., Li, N., and Zeng, R. J. (2016). Cr(VI) reduction
1208 coupled with anaerobic oxidation of methane in a laboratory reactor. *Water Res* 102,
1209 445–452. doi:10/f8zt4f.

1210 Luef, B., Frischkorn, K. R., Wrighton, K. C., Holman, H.-Y. N., Birarda, G., Thomas, B. C.,
1211 et al. (2015). Diverse uncultivated ultra-small bacterial cells in groundwater. *Nat*
1212 *Commun* 6, 6372. doi:10/f634jn.

1213 Luo, Y.-H., Chen, R., Wen, L.-L., Meng, F., Zhang, Y., Lai, C.-Y., et al. (2015). Complete
1214 perchlorate reduction using methane as the sole electron donor and carbon source.
1215 *Environ Sci Technol* 49, 2341–2349. doi:10/f64h36.

1216 Marchler-Bauer, A., Bo, Y., Han, L., He, J., Lanczycki, C. J., Lu, S., et al. (2017).
1217 CDD/SPARCLE: functional classification of proteins via subfamily domain
1218 architectures. *Nucleic Acids Res* 45, D200–D203. doi:10/f9v2z6.

1219 Martínez-Gutiérrez, C. A., Latisnere-Barragán, H., García-Maldonado, J. Q., and López-
1220 Cortés, A. (2018). Screening of polyhydroxyalkanoate-producing bacteria and PhaC-
1221 encoding genes in two hypersaline microbial mats from Guerrero Negro, Baja
1222 California Sur, Mexico. *PeerJ* 6, e4780. doi:10/gddxxn.

1223 Mi, H., Muruganujan, A., and Thomas, P. D. (2013). PANTHER in 2013: modeling the
1224 evolution of gene function, and other gene attributes, in the context of phylogenetic
1225 trees. *Nucleic Acids Res* 41, D377–D386. doi:10/gftg3k.

1226 Mills, H. J., Hodges, C., Wilson, K., MacDonald, I. R., and Sobecky, P. A. (2003). Microbial
1227 diversity in sediments associated with surface-breaching gas hydrate mounds in the
1228 Gulf of Mexico. *FEMS Microbiol Ecol* 46, 39–52. doi:10/bnvmz7.

1229 Minh, B. Q., Nguyen, M. A. T., and von Haeseler, A. (2013). Ultrafast approximation for
1230 phylogenetic bootstrap. *Mol Biol Evol* 30, 1188–1195. doi:10/f3smfd.

1231 Nguyen, L.-T., Schmidt, H. A., von Haeseler, A., and Minh, B. Q. (2015). IQ-TREE: A Fast
1232 and Effective Stochastic Algorithm for Estimating Maximum-Likelihood Phylogenies.
1233 *Mol Biol Evol* 32, 268–274. doi:10/f3srtd.

1234 Ondov, B. D., Treangen, T. J., Melsted, P., Mallonee, A. B., Bergman, N. H., Koren, S., et al.
1235 (2016). Mash: fast genome and metagenome distance estimation using MinHash.
1236 *Genome Biol* 17, 132. doi:10/gfx74q.

1237 Oren, A., Elevi Bardavid, R., and Mana, L. (2014). Perchlorate and halophilic prokaryotes:
1238 implications for possible halophilic life on Mars. *Extremophiles* 18, 75–80.
1239 doi:10/f5mbzb.

1240 Oren, A., and Garrity, G. M. (2018). Uncultivated microbes—in need of their own
1241 nomenclature? *ISME J* 12, 309–311. doi:10/gf7fsc.

1242 Parks, D. H., Chuvochina, M., Chaumeil, P.-A., Rinke, C., Mussig, A. J., and Hugenholtz, P.
1243 (2020). A complete domain-to-species taxonomy for Bacteria and Archaea. *Nat*
1244 *Biotech*, 1–8. doi:10/ggtbk2.

1245 Parks, D. H., Chuvochina, M., Waite, D. W., Rinke, C., Skarshewski, A., Chaumeil, P.-A., et
1246 al. (2018). A standardized bacterial taxonomy based on genome phylogeny
1247 substantially revises the tree of life. *Nat Biotechnol* 36, 996–1004. doi:10/gffzgd.

1248 Parks, D. H., Imelfort, M., Skennerton, C. T., Hugenholtz, P., and Tyson, G. W. (2015).
1249 CheckM: assessing the quality of microbial genomes recovered from isolates, single
1250 cells, and metagenomes. *Genome Res* 25, 1043–1055. doi:10/bb8q.

1251 Parks, D. H., Rinke, C., Chuvochina, M., Chaumeil, P.-A., Woodcroft, B. J., Evans, P. N., et
1252 al. (2017). Recovery of nearly 8,000 metagenome-assembled genomes substantially
1253 expands the tree of life. *Nat Microbiol* 2, 1533–1542. doi:10/cczd.

Payne, T. E. (2012). Background report on the Little Forest Burial Ground legacy waste site. Lucas Heights, N.S.W. (AU): Institute for Environmental Research, Australian Nuclear Science and Technology Organisation Available at: http://apo.ansto.gov.au/dspace/handle/10238/4473 [Accessed July 8, 2016].

Payne, T. E., Harrison, J. J., Cendon, D. I., Comarmond, M. J., Hankin, S., Hughes, C. E., et al. (2020). Radionuclide distributions and migration pathways at a legacy trench disposal site. *J Environ Radioact* 211, 106081. doi:10/ghnj86.

Payne, T. E., Harrison, J. J., Hughes, C. E., Johansen, M. P., Thiruvoth, S., Wilsher, K. L., et al. (2013). Trench 'bathtubbing' and surface plutonium contamination at a legacy radioactive waste site. *Environ Sci Technol* 47, 13284–13293. doi:10/f5kd8g.

Pedruzzi, I., Rivoire, C., Auchincloss, A. H., Coudert, E., Keller, G., de Castro, E., et al. (2015). HAMAP in 2015: updates to the protein family classification and annotation system. *Nucleic Acids Res* 43, D1064–D1070. doi:10/f64sgw.

Price, M. N., Dehal, P. S., and Arkin, A. P. (2010). FastTree 2 – Approximately Maximum-Likelihood Trees for Large Alignments. *PLoS ONE* 5, e9490. doi:10/cfmfnh.

Pritchard, L., Glover, R. H., Humphris, S., Elphinstone, J. G., and Toth, I. K. (2015). Genomics and taxonomy in diagnostics for food security: soft-rotting enterobacterial plant pathogens. *Anal Methods* 8, 12–24. doi:10/ggbwwb.

Probst, A. J., Ladd, B., Jarett, J. K., Geller-McGrath, D. E., Sieber, C. M. K., Emerson, J. B., et al. (2018). Differential depth distribution of microbial function and putative symbionts through sediment-hosted aquifers in the deep terrestrial subsurface. *Nat Microbiol* 3, 328–336. doi:10/gc6xwj.

Rawlings, N. D., Waller, M., Barrett, A. J., and Bateman, A. (2014). MEROPS: the database of proteolytic enzymes, their substrates and inhibitors. *Nucleic Acids Res* 42, D503–D509. doi:10/f5snh7.

Reddy, C. S. K., Ghai, R., Rashmi, and Kalia, V. C. (2003). Polyhydroxyalkanoates: an overview. *Bioresour Technol* 87, 137–146. doi:10/cc2bbd.

Reeburgh, W. S. (2007). Oceanic methane biogeochemistry. *Chem Rev* 107, 486–513. doi:10/bchngf.

Rinke, C., Chuvochina, M., Mussig, A. J., Chaumeil, P.-A., Waite, D. W., Whitman, W. B., et al. (2020). A rank-normalized archaeal taxonomy based on genome phylogeny resolves widespread incomplete and uneven classifications. *bioRxiv*, 2020.03.01.972265. doi:10/ggxwhh.

Rinke, C., Schwientek, P., Sczyrba, A., Ivanova, N. N., Anderson, I. J., Cheng, J.-F., et al. (2013). Insights into the phylogeny and coding potential of microbial dark matter. *Nature* 499, 431–437. doi:10/f45hdq.

Rohart, F., Gautier, B., Singh, A., and Cao, K.-A. L. (2017). mixOmics: An R package for 'omics feature selection and multiple data integration. *PLoS Comput Biol* 13, e1005752. doi:10/gcj84s.

Rosselló-Móra, R., and Whitman, W. B. (2019). Dialogue on the nomenclature and classification of prokaryotes. *Syst Appl Microbiol* 42, 5–14. doi:10/gdz67d.

Saier, M. H., Reddy, V. S., Tamang, D. G., and Västermark, Å. (2014). The Transporter Classification Database. *Nucleic Acids Res* 42, D251–D258. doi:10/gf5c6x.

Seemann, T. (2014). Prokka: rapid prokaryotic genome annotation. *Bioinformatics* 30, 2068–2069. doi:10/f6b3k4.

Servant, F., Bru, C., Carrère, S., Courcelle, E., Gouzy, J., Peyruc, D., et al. (2002). ProDom: Automated clustering of homologous domains. *Brief Bioinform* 3, 246–251. doi:10/c7khjj.

Shen, H., and Huang, J. Z. (2008). Sparse principal component analysis via regularized low rank matrix approximation. *J Multivar Anal* 99, 1015–1034. doi:10/b7x3cc.

Sigrist, C. J. A., Castro, E. de, Cerutti, L., Cuche, B. A., Hulo, N., Bridge, A., et al. (2013). New and continuing developments at PROSITE. *Nucleic Acids Res* 41, D344–D347. doi:10/ggbwr7.

Sivan, O., Antler, G., Turchyn, A. V., Marlow, J. J., and Orphan, V. J. (2014). Iron oxides stimulate sulfate-driven anaerobic methane oxidation in seeps. *PNAS* 111, E4139–E4147. doi:10/f6j76w.

Song, G. C., Im, H., Jung, J., Lee, S., Jung, M.-Y., Rhee, S.-K., et al. (2019). Plant growth-promoting archaea trigger induced systemic resistance in *Arabidopsis thaliana* against *Pectobacterium carotovorum* and *Pseudomonas syringae*. *Environ Microbiol* 21, 940–948. doi:10/gfvmv3.

Spang, A., Poehlein, A., Offre, P., Zumbrägel, S., Haider, S., Rychlik, N., et al. (2012). The genome of the ammonia-oxidizing *Candidatus* Nitrososphaera gargensis: insights into metabolic versatility and environmental adaptations. *Environ Microbiol* 14, 3122–3145. doi:10/f3sp9r.

Tang, X., Zheng, H., Teng, H., Sun, Y., Guo, J., Xie, W., et al. (2016). Chemical coagulation process for the removal of heavy metals from water: a review. *Desalin Water Treat* 57, 1733–1748. doi:10/gg78r6.

Vaksmaa, A., Guerrero-Cruz, S., van Alen, T. A., Cremers, G., Ettwig, K. F., Lüke, C., et al. (2017). Enrichment of anaerobic nitrate-dependent methanotrophic '*Candidatus* Methanoperedens nitroreducens' archaea from an Italian paddy field soil. *Appl Microbiol Biotechnol* 101, 7075–7084. doi:10/gbv5qk.

van Dongen, S., and Abreu-Goodger, C. (2012). "Using MCL to Extract Clusters from Networks," in *Bacterial Molecular Networks: Methods and Protocols* Methods in Molecular Biology., eds. J. van Helden, A. Toussaint, and D. Thieffry (New York, NY: Springer New York), 281–295. doi:10.1007/978-1-61779-361-5_15.

Vázquez-Campos, X., Kinsela, A. S., Bligh, M., Harrison, J. J., Payne, T. E., and Waite, T. D. (2017). Response of microbial community function to fluctuating geochemical conditions within a legacy radioactive waste trench environment. *Appl Environ Microbiol* 83, e00729. doi:10/gf6b7d.

Wang, H. C., Minh, B. Q., Susko, S., and Roger, A. J. (2018). Modeling site heterogeneity with posterior mean site frequency profiles accelerates accurate phylogenomic estimation. *Syst Biol* 67, 216–235. doi:10/gbx7j2.

Waters, E., Hohn, M. J., Ahel, I., Graham, D. E., Adams, M. D., Barnstead, M., et al. (2003). The genome of *Nanoarchaeum equitans*: Insights into early archaeal evolution and derived parasitism. *PNAS* 100, 12984–12988. doi:10/b7zg4c.

Whitman, W. B. (2016). Modest proposals to expand the type material for naming of prokaryotes. *Int J Syst Evol Microbiol* 66, 2108–2112. doi:10/f8nd54.

Wu, C. H., Nikolskaya, A., Huang, H., Yeh, L.-S. L., Natale, D. A., Vinayaka, C. R., et al. (2004). PIRSF: family classification system at the Protein Information Resource. *Nucleic Acids Res* 32, D112–D114. doi:10/bsc8q8.

Wu, M., Luo, J.-H., Hu, S., Yuan, Z., and Guo, J. (2019). Perchlorate bio-reduction in a methane-based membrane biofilm reactor in the presence and absence of oxygen. *Water Res* 157, 572–578. doi:10/gf4kxx.

Xie, T., Yang, Q., Winkler, M. K. H., Wang, D., Zhong, Y., An, H., et al. (2018). Perchlorate bioreduction linked to methane oxidation in a membrane biofilm reactor: Performance and microbial community structure. *J Hazard Mater* 357, 244–252. doi:10/gd395g.

Xu, S., Dai, Z., Guo, P., Fu, X., Liu, S., Zhou, L., et al. (2021). ggtreeExtra: Compact visualization of richly annotated phylogenetic data. *Molecular Biology and Evolution*. doi:10/gkgbpf.

Yamada, K. D., Tomii, K., and Katoh, K. (2016). Application of the MAFFT sequence alignment program to large data—reexamination of the usefulness of chained guide trees. *Bioinformatics* 32, 3246–3251. doi:10/gbrb3f.

Yin, Y., Mao, X., Yang, J., Chen, X., Mao, F., and Xu, Y. (2012). dbCAN: a web resource for automated carbohydrate-active enzyme annotation. *Nucleic Acids Res* 40, W445–W451. doi:10/f35rsw.

Yoshimatsu, K., Sakurai, T., and Fujiwara, T. (2000). Purification and characterization of dissimilatory nitrate reductase from a denitrifying halophilic archaeon, *Haloarcula marismortui*. *FEBS Lett* 470, 216–220. doi:10/bndxqz.

Youssef, N. H., Rinke, C., Stepanauskas, R., Farag, I., Woyke, T., and Elshahed, M. S. (2015). Insights into the metabolism, lifestyle and putative evolutionary history of the novel archaeal phylum 'Diapherotrites.' *ISME J* 9, 447–460. doi:10/gfb6wp.

Yu, G. (2020). Using ggtree to Visualize Data on Tree-Like Structures. *Curr Protoc Bioinformatics* 69, e96. doi:10/gh3fpj.

Yu, N. Y., Wagner, J. R., Laird, M. R., Melli, G., Rey, S., Lo, R., et al. (2010). PSORTb 3.0: improved protein subcellular localization prediction with refined localization subcategories and predictive capabilities for all prokaryotes. *Bioinformatics* 26, 1608–1615. doi:10/bz3q2w.

Yutin, N., Puigbò, P., Koonin, E. V., and Wolf, Y. I. (2012). Phylogenomics of prokaryotic ribosomal proteins. *PLOS ONE* 7, e36972. doi:10/ggbwtp.

Zaremba-Niedzwiedzka, K., Caceres, E. F., Saw, J. H., Bäckström, D., Juzokaite, L., Vancaester, E., et al. (2017). Asgard archaea illuminate the origin of eukaryotic cellular complexity. *Nature* 541, 353–358. doi:10/f9kz9q.

Zhang, C., Rabiee, M., Sayyari, E., and Mirarab, S. (2018). ASTRAL-III: polynomial time species tree reconstruction from partially resolved gene trees. *BMC Bioinformatics* 19, 153. doi:10/gfzph7.

1380 # Figures and tables

1381 **Table 1**. Summary of new taxa proposed. Formal descriptions of the taxa in this table are
1382 included in the Taxonomic Appendix with additional details on the proposed type materials in
1383 Table S6.

1384 **Table 2**. General characteristics of the genomes reconstructed in this study. MAGs in bold
1385 indicate named candidate species (see Table 1). Additional details can be found in Table S7.
1386 Expanded completeness analysis are available in Table S8.

1387 **Figure 1**. Phylogenomic analysis of the archaeal MAGs found at LFLS. Concatenated protein
1388 tree constructed with 44 universal and Archaea-specific ribosomal proteins from 230 reference
1389 genomes and 36 original MAGs from this work. Tree was constructed with IQ-TREE under
1390 the PMSF+LG+C60+F+I+G. Lineages with representatives at LFLS are shown coloured and
1391 uncollapsed, with labels in blue. Inner ring indicates the major archaeal lineages. Shortened
1392 branches are shown at 50% of their length. Black circles indicate ultrafast bootstrap support
1393 values >90%.

1394 **Figure 2**. Abundance of MEROPS subfamilies, CAZy families, and biogeochemically relevant
1395 proteins found in the MAGs from LFLS. MAGs are ordered according to the rp44 tree (Figure
1396 1). Counts of each protein are capped at 10 for easier visualisation. Details about MEROPS,
1397 CAZy, and proteins of biogeochemical relevance, including exact counts and classes with
1398 predicted extracellular proteins can be found in Tables S11, S13 and S10, respectively. Plot
1399 created with ggtree v3.1.0 (Yu, 2020) and ggtreeExtra v1.0.4 (Xu et al., 2021).

1400 **Figure 3**. Phylogenomic placement of the *Micrarchaeota* orders and families with respect to
1401 the type family *Micrarchaeaceae*. Subtree extracted from the concatenated DPANN
1402 phylogenomic tree highlighting families and orders. Filled circles indicate UFBoot support ≥

1403 90% in the dpann-concat tree. Scale bar indicates RED. Solid vertical lines indicate minimum
1404 and maximum RED values for order (blue), family (green), and genus (purple). Dashed lines
1405 indicate median RED values.

1406 **Figure 4**. Comparative visualisation of the metabolism of LFWA-III representative MAGs
1407 from this study (green circles) and selected reference DPANN genomes (red circled). Each
1408 sector in the indicative circles indicates the presence or absence of a key protein in the
1409 represented genome. Extracellular enzymes are not shown for simplicity. Abbreviations: 2-OG,
1410 2-oxoglutarate; 2-OIV, 2-oxoisovalerate; AICAR, 5-amino-1-(5-phospho-D-
1411 ribosyl)imidazole-4-carboxamide; AIR, 5-amino-1-(5-phospho-β-D-ribosyl)imidazole; ARP,
1412 5-amino-6-ribitylamino-2,4(1H,3H)-pyrimidinedione; CAIR, 5-amino-1-(5-phospho-D-
1413 ribosyl)imidazole-4-carboxylate; F1,6P, β-D-Fructose 1,6-bisphosphate; F6P, β-D-Fructose-
1414 6P; FAD, Flavin adenine dinucleotide; FMN, Flavin mononucleotide; G3P, Glyceraldehyde-
1415 3P; G6P, Glucose-6P; Gluc6P: D-gluconate 6-phosphate; GlucL6P: D-glucono-1,5-lactone 6-
1416 phosphate; GP, Glycerone-P; HMP-PP, 4-amino-5-hydroxymethyl-2-methylpyrimidine
1417 diphosphate; IOR: indolepyruvate:ferredoxin oxidoreductase; KOR: 2-oxoglutarate:ferredoxin
1418 oxidoreductase; LDH: D-lactate dehydrogenase (NAD^+); N5-CAIR, 5-
1419 (carboxyamino)imidazole ribonucleotide; NAD^+, β-nicotinamide adenine dinucleotide;
1420 $NADP^+$, β-nicotinamide adenine dinucleotide phosphate; NMN, β-nicotinamide D-
1421 ribonucleotide; OAA, Oxaloacetate; OAHS, O-acetyl-homoserine; OFOR: 2-
1422 oxoacid:ferredoxin oxidoreductase; OSHS, O-succinyl-homoserine; PEP,
1423 Phosphoenolpyruvate; POR: pyruvate:ferredoxin oxidoreductase; PRPP, 5-phospho-α-D-
1424 ribose 1-diphosphate; Ru5P, D-ribulose 5-phosphate; SAH, S-adenosyl-L-homocysteine;
1425 SAM, S-adenosyl-L-methionine; ThDP, Thiamine diphosphate; ThMP, Thiamine
1426 monophosphate; THZ, 4-methyl-5-(β-hydroxyethyl)thiazolium; THZ-P, 4-methyl-5-(β-
1427 hydroxyethyl)thiazolium phosphate.

1428 **Figure 5**. sPCA analysis of the functional (A) and compositional (B) features in DPANN
1429 genomes. Only explanatory variables correlated at absolute value of ≥ 0.75 with the principal
1430 components are shown. Variables are scaled (4x) for easier visualisation. MAGs from LFLS
1431 lineages are displayed with larger circles.

1432 **Figure 6**. Pangenomic analysis of genus *Methanoperedens*. Pangenome was generated with 6
1433 *Methanoperedens* spp. MAGs from LFLS (pink) and 4 reference genomes (blue), accounting
1434 for a total of 31,974 protein-coding genes grouped in 10,525 gene clusters. Gene clusters
1435 generated with an MCL inflation value of 6.0.

1436 **Figure 7**. Phylogenetic analysis of molybdopterin oxidoreductase proteins. Tree was generated
1437 with 268 reference sequences and 8 query sequences from '*Ca.* Methanoperedens' spp. NarG(-
1438 like) proteins. Tree was built under model LG+R10 model and 10,000 ultrafast bootstrap
1439 iterations. Branches with ultrafast bootstrap support values <50% are collapsed. Black circles
1440 indicate a branch support ≥90%.

Table 1. Summary of new taxa proposed. Formal descriptions of the taxa in this table are included in the Taxonomic Appendix with additional details on the proposed type materials in Table S6.

Phylum	Class	Order	Family	Genus	Species	Type
Nanoarchaeota	"Nanoarchaeia" class. nov. [a]	'*Ca*. Tiddalikarchaeales' ord. nov.	'*Ca*. Tiddalikarchaeaceae' fam. nov.	'*Ca*. Tiddalikarchaeum' gen. nov.	'*Ca*. Tiddalikarchaeum anstoanum' sp. nov.	LFW-252_1 [b]
Micrarchaeota	'*Ca*. Micrarchaeia' class. nov. [a]	'*Ca*. Micrarchaeales' ord. nov. [a]	'*Ca*. Micrarchaeaceae' fam. nov. [a]	'*Ca*. Micrarchaeum'	'*Ca*. Micrarchaeum acidiphilum'	
		'*Ca*. Norongarragalinales' ord. nov.	'*Ca*. Norongarragalinaceae' fam. nov.	'*Ca*. Norongarragalina' gen. nov.	'*Ca*. Norongarragalina meridionalis' sp. nov.	LFW-144_1 [b]
		'*Ca*. Gugararchaeales' ord. nov.	'*Ca*. Gugararchaeaceae' fam. nov.	'*Ca*. Gugararchaeum' gen. nov.	'*Ca*. Gugararchaeum adminiculabundum' sp. nov.	LFW-121_3 [b]
			'*Ca*. Burarchaeaceae' fam. nov.	'*Ca*. Burarchaeum' gen. nov.	'*Ca*. Burarchaeum australiense' sp. nov.	LFW-281_7 [b]
		'*Ca*. Anstonellales' ord. nov.	'*Ca*. Anstonellaceae' fam. nov.	'*Ca*. Anstonella' gen. nov.	'*Ca*. Anstonella stagnisolia' sp. nov.	LFW-35 [b]
			'*Ca*. Bilamarchaeaceae' fam. nov.	'*Ca*. Bilamarchaeum' gen. nov.	'*Ca*. Bilamarchaeum dharawalense' sp. nov.	LFW-283_2 [b]
Euryarchaeota [d]	Methanomicrobia [d]	Methanosarcinales	'*Ca*. Methanoperedenaceae'	'*Ca*. Methanoperedens'	'*Ca*. Methanoperedens vercellense' sp. nov. [c]	'*Ca*. Methanoperedens nitroreducens' Vercelli
					'*Ca*. Methanoperedens batavicum' sp. nov. [c]	'*Ca*. Methanoperedens nitroreducens' BLZ1 (or MPEBLZ)

[a]: new proposal to fill gaps in taxonomic ranks.

[b]: obtained in this study.

[c]: based on extant data used in this work.

[d]: Phylum p__Halobacterota, class c__Methanosarcinia according to GTDB.

Table 2. General characteristics of the genomes reconstructed in this study. MAGs in bold indicate named candidate species (see Table 1). Additional details can be found in Table S7. Expanded completeness analysis is available in Table S8.

MAG	Lineage	Contigs	Size (Mbp)	tRNA[a]	GC (%)	rRNA genes[b]	C% / R%[c]
LFW-28	Altiarchaeota	151	2.41	23	49.9	Y/N/Y	92.6 / 0[e]
LFW-252_2	Diapherotrites	64	1.05	21	40.6	Y/Y/Y	91.4 / 3.2
LFW-281_4	Diapherotrites	72	1.09	20	49.7	Y/Y/Y	71 / 5.4
LFW-252_1	LFWA-I	56	1.16	21	36.5	Y/Y/Y	95.7 / 1.1
LFW-144_1	LFWA-II	49	0.93	20	57.5	Y/N/Y	93.5 / 1.1
LFW-156_1	LFWA-II	109	0.93	18	32.5	N/N/Y	90.3 / 8.6
LFW-121_3	LFWA-IIIa	76	1.47	21	49.8	Y/Y/Y	96.8 / 2.2
LFW-281_7	LFWA-IIIa	76	1.20	18	57.6	Y/N/Y	96.8 / 5.4
LFW-144_2_1	LFWA-IIIa	219	0.77	16	57.5	N/N/N	52.7 / 0
LFW-281_1_2	LFWA-IIIb	79	0.71	17	55.7	N/N/Y	50 / 2.5 [e]
LFW-283_2	LFWA-IIIb	63	1.27	20	40.0	Y/Y/Y	95.7 / 0
LFW-281_3_2	LFWA-IIIb	81	1.08	19	54.9	N/N/Y	78.5 / 6.5
LFW-281_5_4	LFWA-IIIb	104	0.64	15	55.4	N/N/Y	63.4 / 9.7
LFW-281_6_1	LFWA-IIIb	122	0.70	14	53.7	N/Y/N	59.1 / 9.7
LFW-29	LFWA-IIIb	68	1.30	21	62.2	N/N/Y	97.8 / 0
LFW-35	LFWA-IIIb	68	1.33	21	50.3	Y/Y/Y	97.8 / 2.2
LFW-242_1	LFWA-III related[d]	69	0.97	21	57.3	N/N/Y	93.5 / 6.5
LFW-46	LFWA-IV	85	1.20	18	43.8	N/N/Y	92.5 / 3.2
LFW-125_1	Micrarchaeales	97	0.82	20	54.7	Y/Y/N	84.9 / 0
LFW-165_1	Pacearchaeota	67	1.34	19	30.7	N/N/Y	94.6 / 0
LFW-170_1	Pacearchaeota	42	0.84	19	33.8	Y/Y/Y	91.4 / 0
LFW-170_3	Pacearchaeota	31	0.59	20	35.3	N/N/Y	92.5 / 2.2
LFW-262_2	Pacearchaeota	45	0.62	20	31.5	N/N/Y	74.2 / 8.6
LFW-262_5	Pacearchaeota	44	0.58	19	31.9	N/N/Y	88.2 / 8.6
LFW-273_1	Pacearchaeota	27	0.56	20	33.4	N/N/Y	93.5 / 1.1
LFW-252_3	Woesearchaeota	101	1.04	20	42.3	N/N/Y	90.3 / 2.2
LFW-24	Methanoperedenaceae	169	2.92	21	40.3	N/N/Y	97.4 / 1.3
LFW-280_1_1	Methanoperedenaceae	207	1.69	20	44.4	N/N/N	56.9 / 0.7
LFW-280_2_2	Methanoperedenaceae	298	2.20	15	43.6	N/N/Y	73.3 / 4.6
LFW-280_3_1	Methanoperedenaceae	179	3.24	21	43.8	N/N/Y	99.4 / 1.3
LFW-280_3_2	Methanoperedenaceae	147	2.79	19	43.8	N/N/Y	96.1 / 2
LFW-280_4	Methanoperedenaceae	182	2.60	21	42.9	N/N/Y	98.3 / 0.8
LFW-151_1	Methanotrichaceae	401	1.75	15	53.2	N/N/N	63.2 / 4
LFW-151_2	Methanotrichaceae	390	2.28	16	50.6	N/N/Y	81.5 / 3.4
LFW-83_1	Methanotrichaceae	580	2.63	19	47.7	Y/Y/Y	63.1 / 2.6
LFW-68_2	Thermoplasmata	152	2.06	22	38.2	N/N/Y	91.4 / 5.4
LFW-283_4_5	Thaumarchaeota	152	1.15	18	37.0	N/N/N	56.2 / 7.8

[a]: number of different tRNA found (21 includes starting iMet). Additional tRNA may include Sec, Ile2, or undetermined types.

[b]: found rRNA genes, 16S/23S/5S.

[c]: completeness (C%) and redundancy (R%) estimations. Values for DPANN and Thermoplasmata MAGs derived from the DPANN93 marker collection from this manuscript. Estimations for other MAGs obtained with CheckM lineage_wf unless otherwise stated. Additional C%/%R estimations can be found in the SI.

[d]: likely to constitute a member of an undescribed order sister to LFWA-III.

e: based on Rinke et al. (2013)

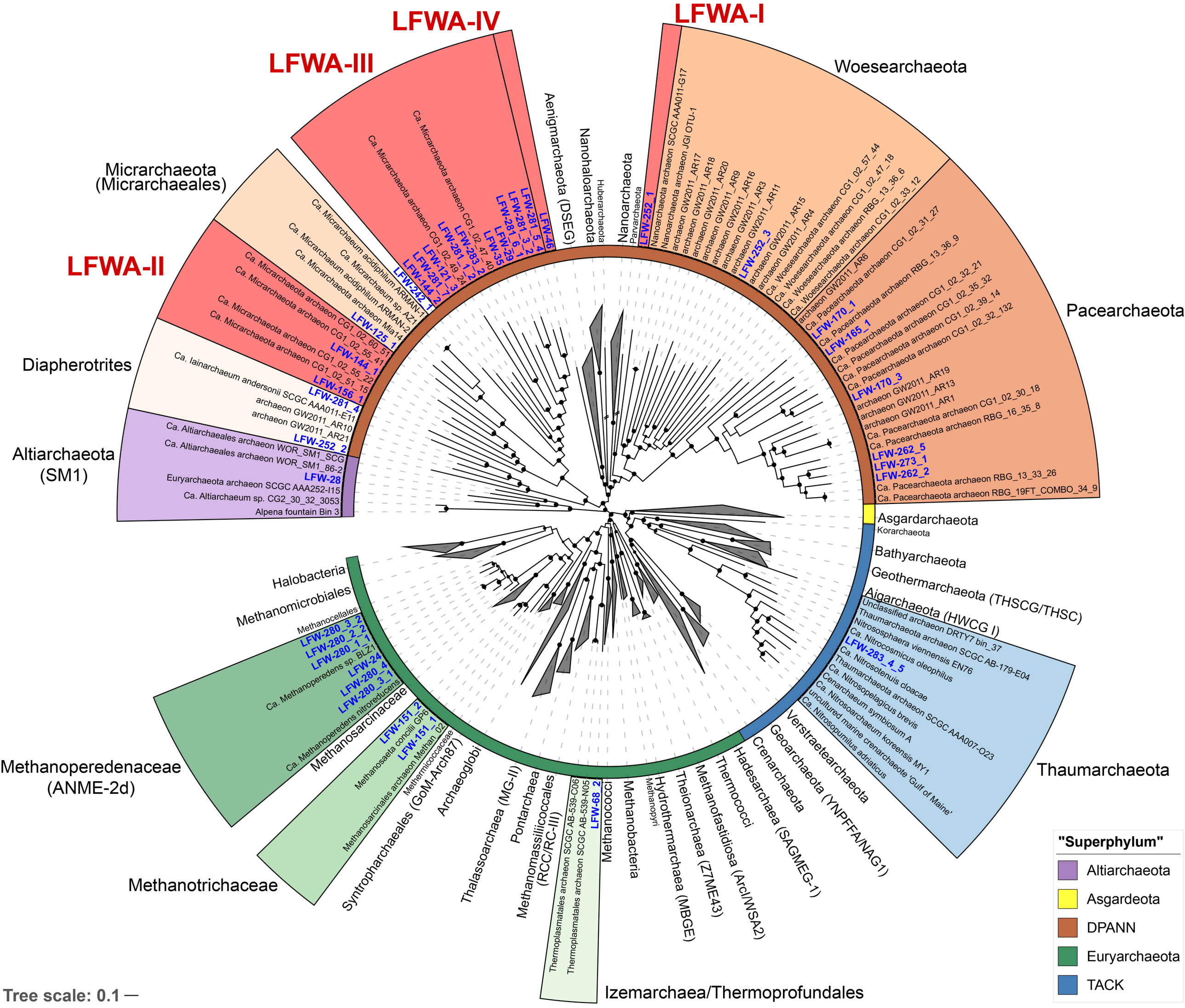
LFWA-IV
LFWA-III
LFWA-I
LFWA-II
Micrarchaeota (Micrarchaeales)
Diapherotrites
Altiarchaeota (SM1)
Aenigmarchaeota (DSEG)
Nanohaloarchaeota
Huberarchaeota
Nanoarchaeota
Parvarchaeota
Woesearchaeota
Pacearchaeota
Asgardarchaeota
Korarchaeota
Bathyarchaeota
Geothermarchaeota (THSCG/THSC)
Aigarchaeota (HWCG I)
Thaumarchaeota
Verstraetearchaeota
Geoarchaeota (YNPFFA/NAG1)
Crenarchaeota
Hadesarchaea (SAGMEG-1)
Thermococci
Methanofastidiosa (Arc/WSA2)
Theionarchaea (Z7ME43)
Hydrothermarchaea (MBGE)
Methanopyri
Methanobacteria
Methanococci
Izemarchaea/Thermoprofundales
Thermoplasmatales archaeon SCGC AB-539-C06
Thermoplasmatales archaeon SCGC AB-539-N05
LFW-68_2
Pontarchaea
Methanomassiliicoccales (RCC/RC-III)
Thalassoarchaea (MG-II)
Archaeoglobi
Syntropharchaeales (GoM-Arch87)
Methanosarcinales archaeon Methan_02
Methermicoccaceae
Methanosaeta concilii GP6
Methanosarcinaceae
Methanotrichaceae
Methanomicrobiales
Methanocellales
Halobacteria
Methanoperedenaceae (ANME-2d)
Ca. Methanoperedens nitroreducens
Ca. Methanoperedens sp. BLZ1
Euryarchaeota archaeon SCGC AAA252-I15
Ca. Altiarchaeum sp. CG2_30_32_3053
Alpena fountain Bin 3
Ca. Altiarchaeales archaeon WOR_SM1_86-2
Ca. Altiarchaeales archaeon WOR_SM1_SCG
Ca. Lainarchaeum andersonii SCGC AAA011-E11
archaeon GW2011_AR10
archaeon GW2011_AR21
Ca. Micrarchaeota archaeon CG1_02_51_15
Ca. Micrarchaeota archaeon CG1_02_55_22
Ca. Micrarchaeota archaeon CG1_02_60_51
Ca. Micrarchaeota archaeon CG1_02_55_41
Ca. Micrarchaeum acidiphilum ARMAN-2
Ca. Micrarchaeum acidiphilum ARMAN-1
Ca. Micrarchaeum sp. AZ1
Ca. Micrarchaeota archaeon Mia14
Ca. Micrarchaeota archaeon CG1_02_47_40
Ca. Micrarchaeota archaeon CG1_02_49_24
Nanoarchaeota archaeon SCGC AAA011-G17
Nanoarchaeota archaeon JGI OTU-1
archaeon GW2011_AR17
archaeon GW2011_AR18
archaeon GW2011_AR20
archaeon GW2011_AR9
archaeon GW2011_AR16
archaeon GW2011_AR3
archaeon GW2011_AR11
archaeon GW2011_AR15
archaeon GW2011_AR4
Ca. Woesearchaeota archaeon CG1_02_57_44
Ca. Woesearchaeota archaeon CG1_02_47_18
Ca. Woesearchaeota archaeon RBG_13_36_6
Ca. Woesearchaeota archaeon CG1_02_33_12
archaeon GW2011_AR6
Ca. Pacearchaeota archaeon CG1_02_31_27
Ca. Pacearchaeota archaeon RBG_13_36_9
Ca. Pacearchaeota archaeon CG1_02_32_21
Ca. Pacearchaeota archaeon CG1_02_35_32
Ca. Pacearchaeota archaeon CG1_02_39_14
Ca. Pacearchaeota archaeon CG1_02_32_132
archaeon GW2011_AR19
archaeon GW2011_AR13
archaeon GW2011_AR1
Ca. Pacearchaeota archaeon CG1_02_30_18
Ca. Pacearchaeota archaeon RBG_16_35_8
Ca. Pacearchaeota archaeon RBG_13_33_26
Ca. Pacearchaeota archaeon RBG_19FT_COMBO_34_9
Unclassified archaeon DRTY7 bin_37
Thaumarchaeota archaeon SCGC AB-179-E04
Nitrosophaera viennensis EN76
Ca. Nitrocosmicus oleophilus
Ca. Nitrosotenuis cloacae
Thaumarchaeota archaeon SCGC AAA007-O23
Ca. Nitrosopelagicus brevis
Cenarchaeum symbiosum A
Ca. Nitrosoarchaeum koreensis MY1
uncultured marine crenarchaeote 'Gulf of Maine'
Ca. Nitrosopumilus adriaticus
LFW-252_1
LFW-252_3
LFW-170_1
LFW-165_1
LFW-170_3
LFW-262_5
LFW-273_1
LFW-262_2
LFW-283_4_5
LFW-280_3_2
LFW-280_2_2
LFW-280_1_1
LFW-24
LFW-280_4
LFW-280_3_1
LFW-151_2
LFW-151_1
LFW-125_1
LFW-144_1
LFW-156_1
LFW-281_4
LFW-252_2
LFW-281_5_4
LFW-281_3_2
LFW-281_6_1
LFW-29
LFW-35
LFW-281_1_2
LFW-283_2
LFW-121_3
LFW-281_7
LFW-144_2
LFW-242_1
LFW-46
"Superphylum"
Altiarchaeota
Asgardeota
DPANN
Euryarchaeota
TACK
Tree scale: 0.1

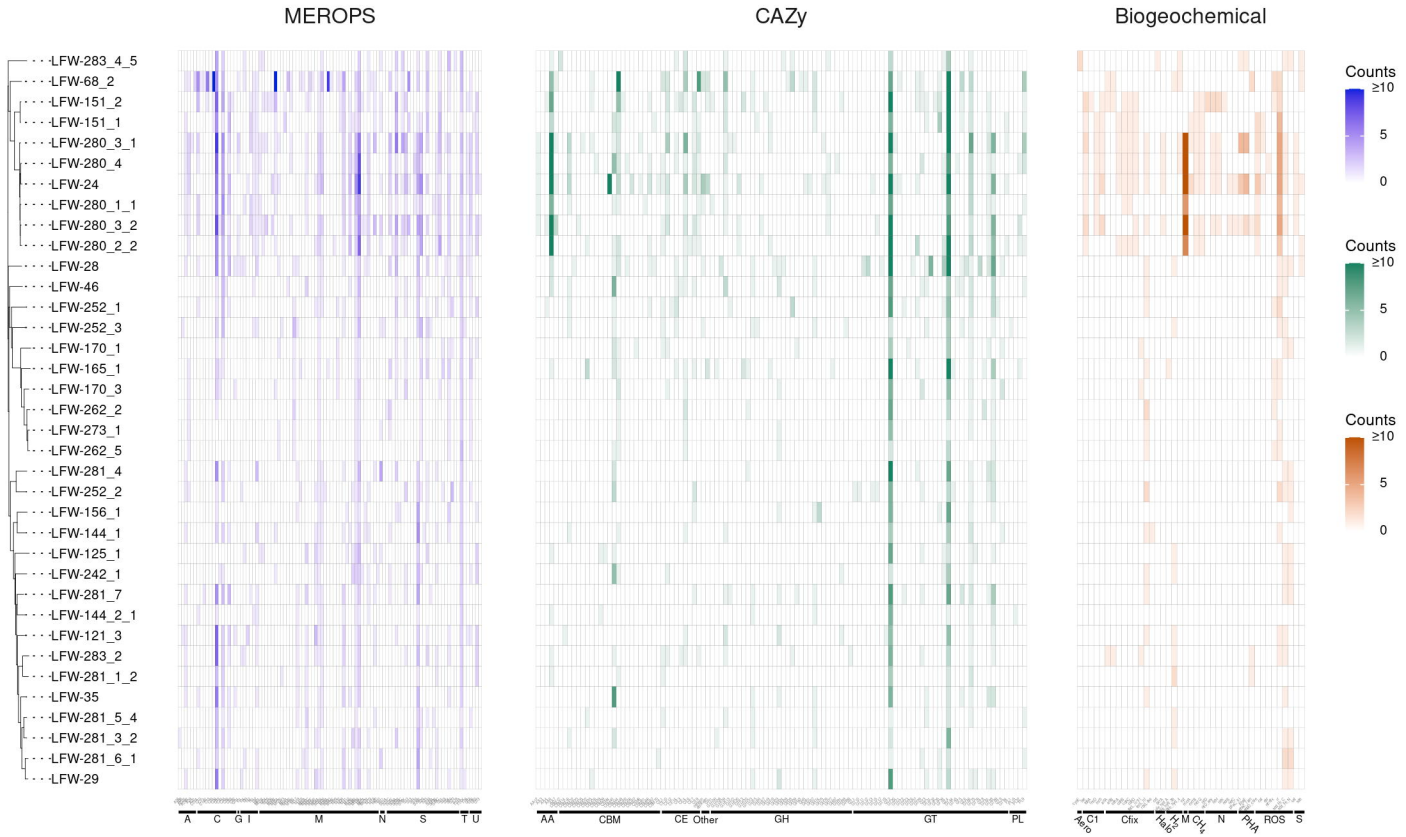
MEROPS
CAZy
Biogeochemical
LFW-283_4_5
LFW-68_2
LFW-151_2
LFW-151_1
LFW-280_3_1
LFW-280_4
LFW-24
LFW-280_1_1
LFW-280_3_2
LFW-280_2_2
LFW-28
LFW-46
LFW-252_1
LFW-252_3
LFW-170_1
LFW-165_1
LFW-170_3
LFW-262_2
LFW-273_1
LFW-262_5
LFW-281_4
LFW-252_2
LFW-156_1
LFW-144_1
LFW-125_1
LFW-242_1
LFW-281_7
LFW-144_2_1
LFW-121_3
LFW-283_2
LFW-281_1_2
LFW-35
LFW-281_5_4
LFW-281_3_2
LFW-281_6_1
LFW-29
A C G I M N S T U
AA CBM CE Other GH GT PL
Aero C1 Cfix Halo H2 M CH4 N PHA ROS S
Counts
≥10
5
0
Counts
≥10
5
0
Counts
≥10
5
0

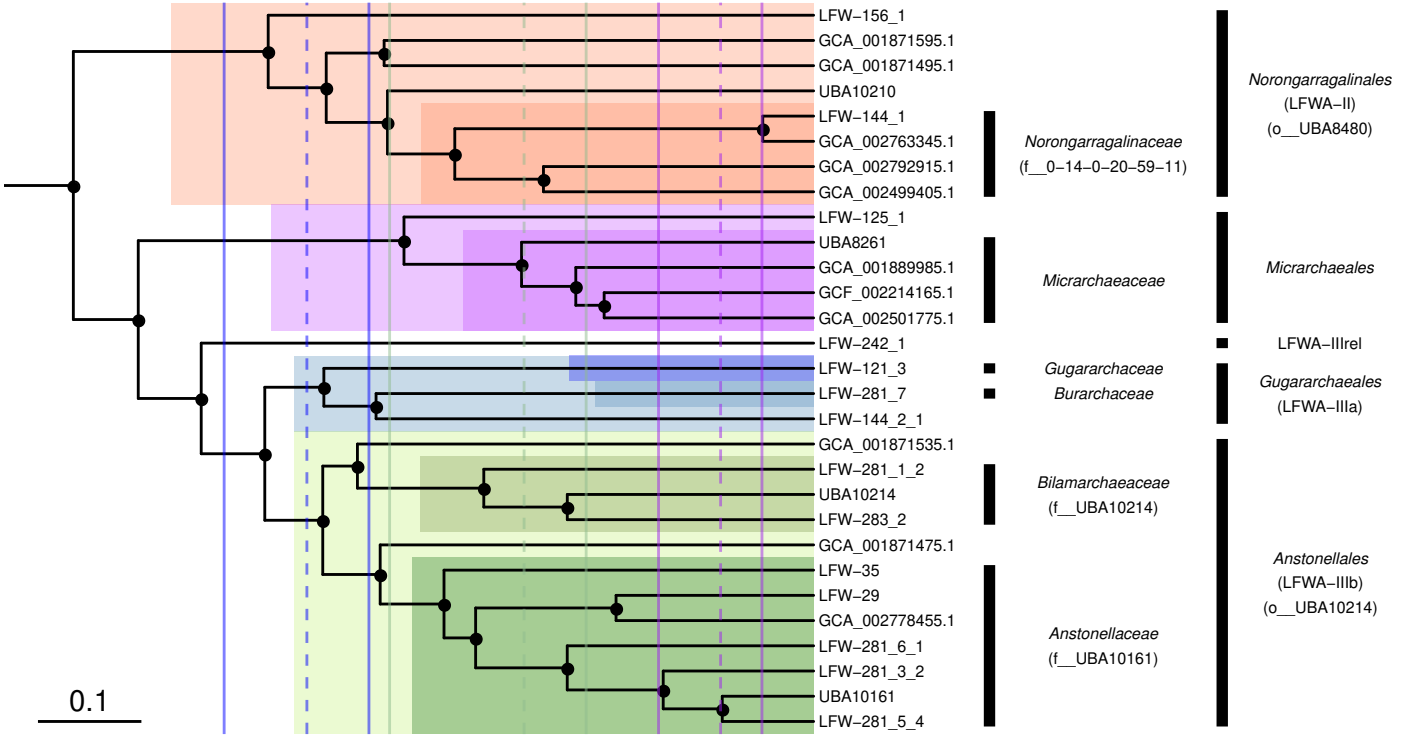
LFW−156_1
GCA_001871595.1
GCA_001871495.1
UBA10210
LFW−144_1
GCA_002763345.1
GCA_002792915.1
GCA_002499405.1
LFW−125_1
UBA8261
GCA_001889985.1
GCF_002214165.1
GCA_002501775.1
LFW−242_1
LFW−121_3
LFW−281_7
LFW−144_2_1
GCA_001871535.1
LFW−281_1_2
UBA10214
LFW−283_2
GCA_001871475.1
LFW−35
LFW−29
GCA_002778455.1
LFW−281_6_1
LFW−281_3_2
UBA10161
LFW−281_5_4
Norongarragalinaceae
(f__0−14−0−20−59−11)
Micrarchaeaceae
Gugararchaceae
Burarchaeaceae
Bilamarchaeaceae
(f__UBA10214)
Anstonellaceae
(f__UBA10161)
Norongarragalinales
(LFWA−II)
(o__UBA8480)
Micrarchaeales
LFWA−IIIrel
Gugararchaeales
(LFWA−IIIa)
Anstonellales
(LFWA−IIIb)
(o__UBA10214)
0.1

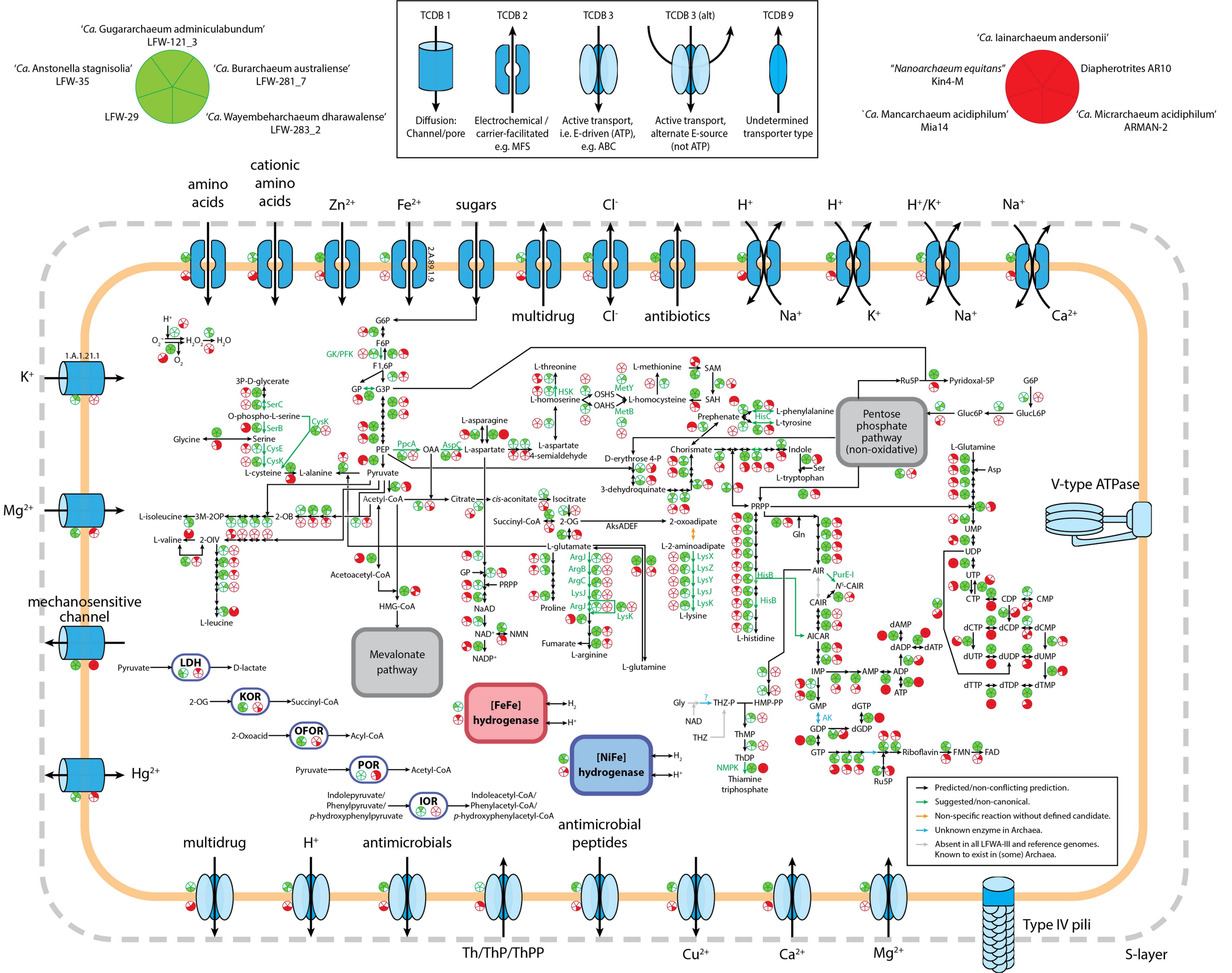
'Ca. Gugararchaeum adminiculabundum' LFW-121_3
'Ca. Anstonella stagnisolia' LFW-35
'Ca. Burarchaeum australiense' LFW-281_7
LFW-29
'Ca. Wayembeharchaeum dharawalense' LFW-283_2
TCDB 1
TCDB 2
TCDB 3
TCDB 3 (alt)
TCDB 9
Diffusion: Channel/pore
Electrochemical / carrier-facilitated e.g. MFS
Active transport, i.e. E-driven (ATP), e.g. ABC
Active transport, alternate E-source (not ATP)
Undetermined transporter type
'Ca. Iainarchaeum andersonii'
"Nanoarchaeum equitans" Kin4-M
Diapherotrites AR10
`Ca. Mancarchaeum acidiphilum' Mia14
'Ca. Micrarchaeum acidiphilum' ARMAN-2
amino acids
cationic amino acids
Zn2+
Fe2+
sugars
Cl-
H+
H+
H+/K+
Na+
multidrug
Cl-
antibiotics
Na+
K+
Na+
Ca2+
2.A.89.1.9
1.A.1.21.1
K+
Mg2+
mechanosensitive channel
Hg2+
V-type ATPase
Pentose phosphate pathway (non-oxidative)
Mevalonate pathway
[FeFe] hydrogenase
[NiFe] hydrogenase
LDH
KOR
OFOR
POR
IOR
multidrug
H+
antimicrobials
antimicrobial peptides
Th/ThP/ThPP
Cu2+
Ca2+
Mg2+
Type IV pili
S-layer
Predicted/non-conflicting prediction.
Suggested/non-canonical.
Non-specific reaction without defined candidate.
Unknown enzyme in Archaea.
Absent in all LFWA-III and reference genomes. Known to exist in (some) Archaea.

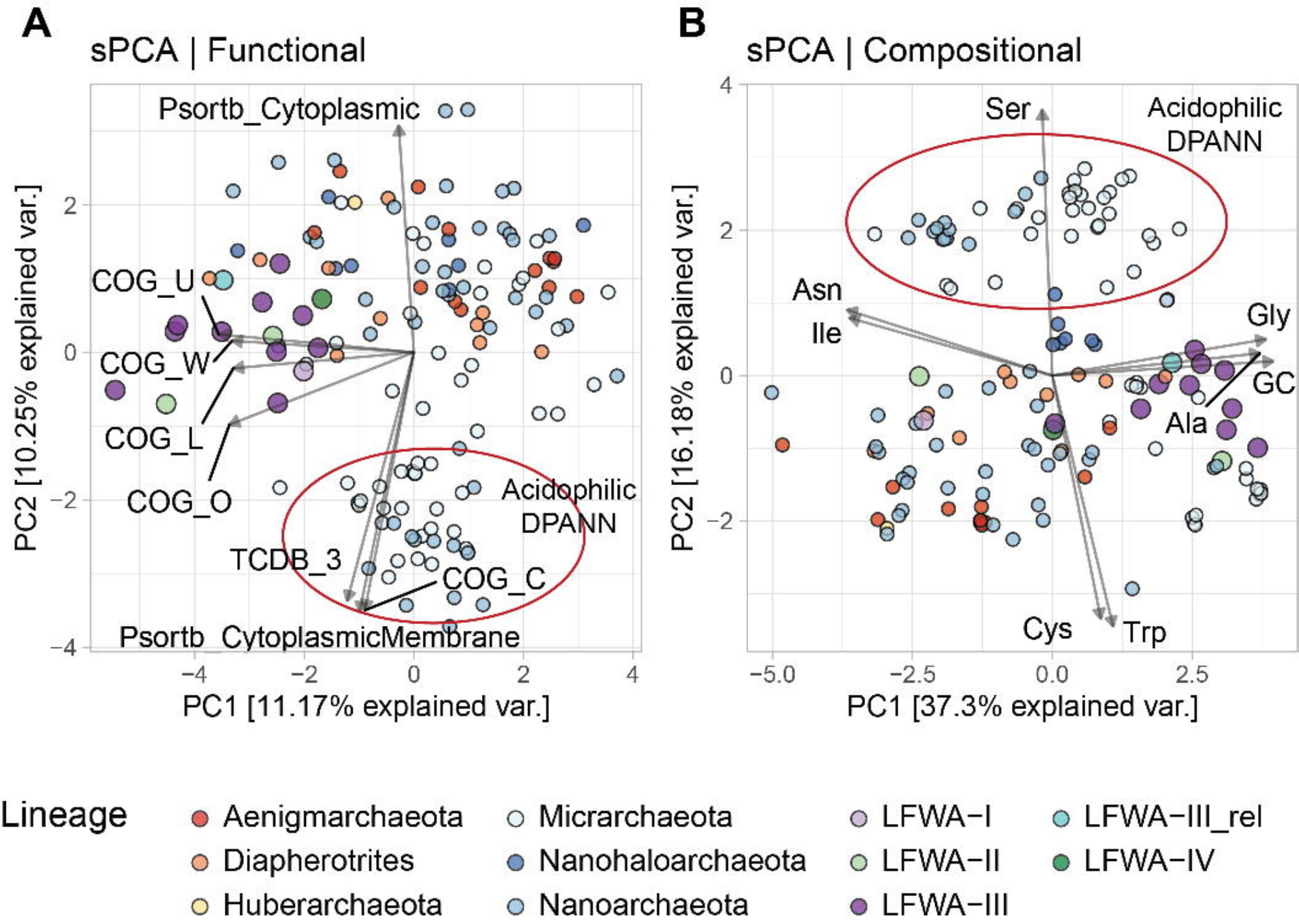
A
sPCA | Functional
Psortb_Cytoplasmic
COG_U
COG_W
COG_L
COG_O
TCDB_3
COG_C
Acidophilic
DPANN
Psortb_CytoplasmicMembrane
PC2 [10.25% explained var.]
PC1 [11.17% explained var.]
B
sPCA | Compositional
Ser
Acidophilic
DPANN
Asn
Ile
Gly
GC
Ala
Cys
Trp
PC2 [16.18% explained var.]
PC1 [37.3% explained var.]
Lineage
Aenigmarchaeota
Diapherotrites
Huberarchaeota
Micrarchaeota
Nanohaloarchaeota
Nanoarchaeota
LFWA−I
LFWA−II
LFWA−III
LFWA−III_rel
LFWA−IV

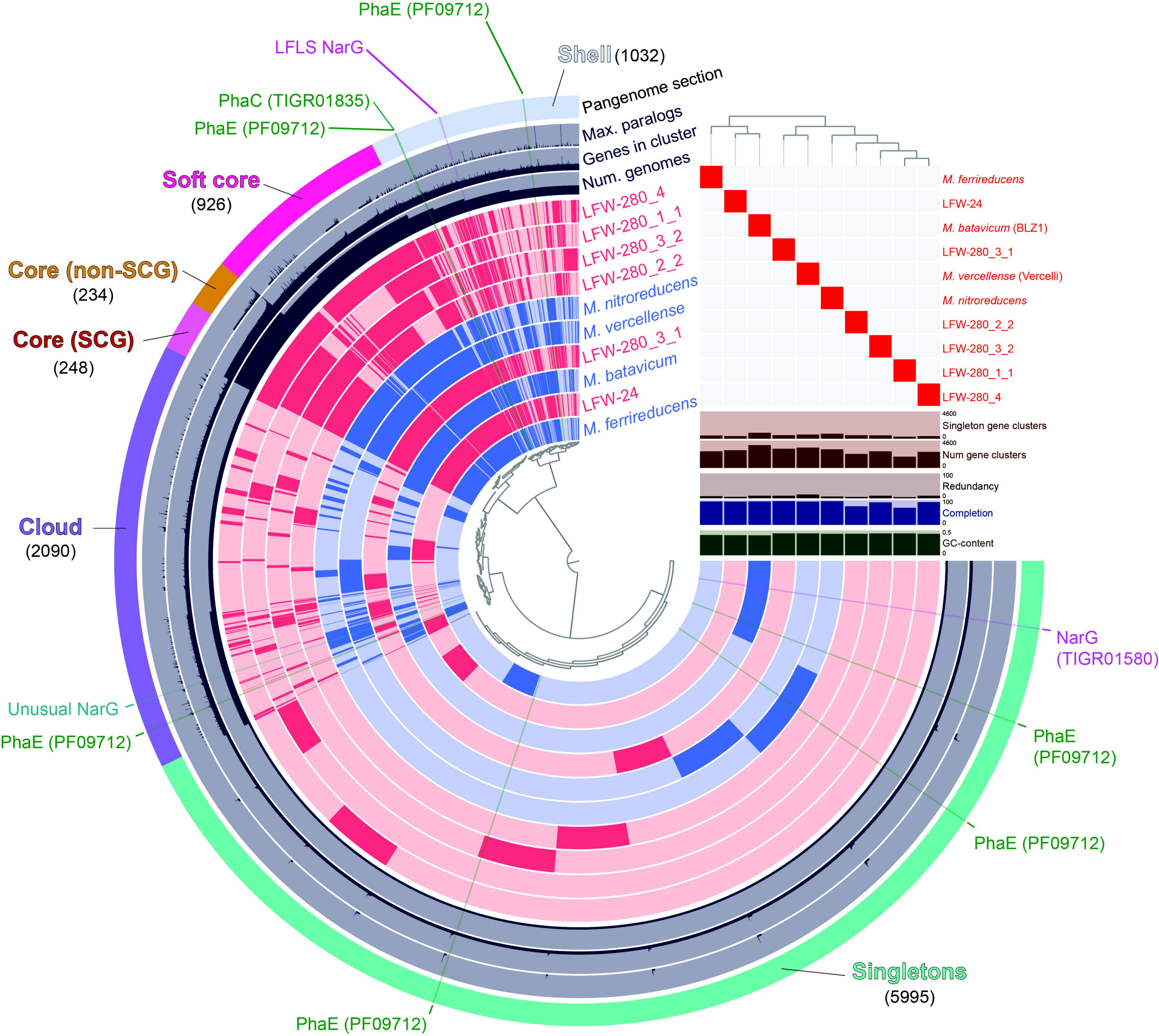
PhaE (PF09712)
LFLS NarG
Shell (1032)
PhaC (TIGR01835)
PhaE (PF09712)
Pangenome section
Max. paralogs
Genes in cluster
Num. genomes
Soft core
(926)
Core (non-SCG)
(234)
Core (SCG)
(248)
Cloud
(2090)
LFW-280_4
LFW-280_1_1
LFW-280_3_2
LFW-280_2_2
M. nitroreducens
M. vercellense
LFW-280_3_1
M. batavicum
LFW-24
M. ferrireducens
M. ferrireducens
LFW-24
M. batavicum (BLZ1)
LFW-280_3_1
M. vercellense (Vercelli)
M. nitroreducens
LFW-280_2_2
LFW-280_3_2
LFW-280_1_1
LFW-280_4
4600
Singleton gene clusters
0
4600
Num gene clusters
0
100
Redundancy
0
100
Completion
0
0.5
GC-content
0
NarG
(TIGR01580)
Unusual NarG
PhaE (PF09712)
PhaE
(PF09712)
PhaE (PF09712)
Singletons
(5995)
PhaE (PF09712)

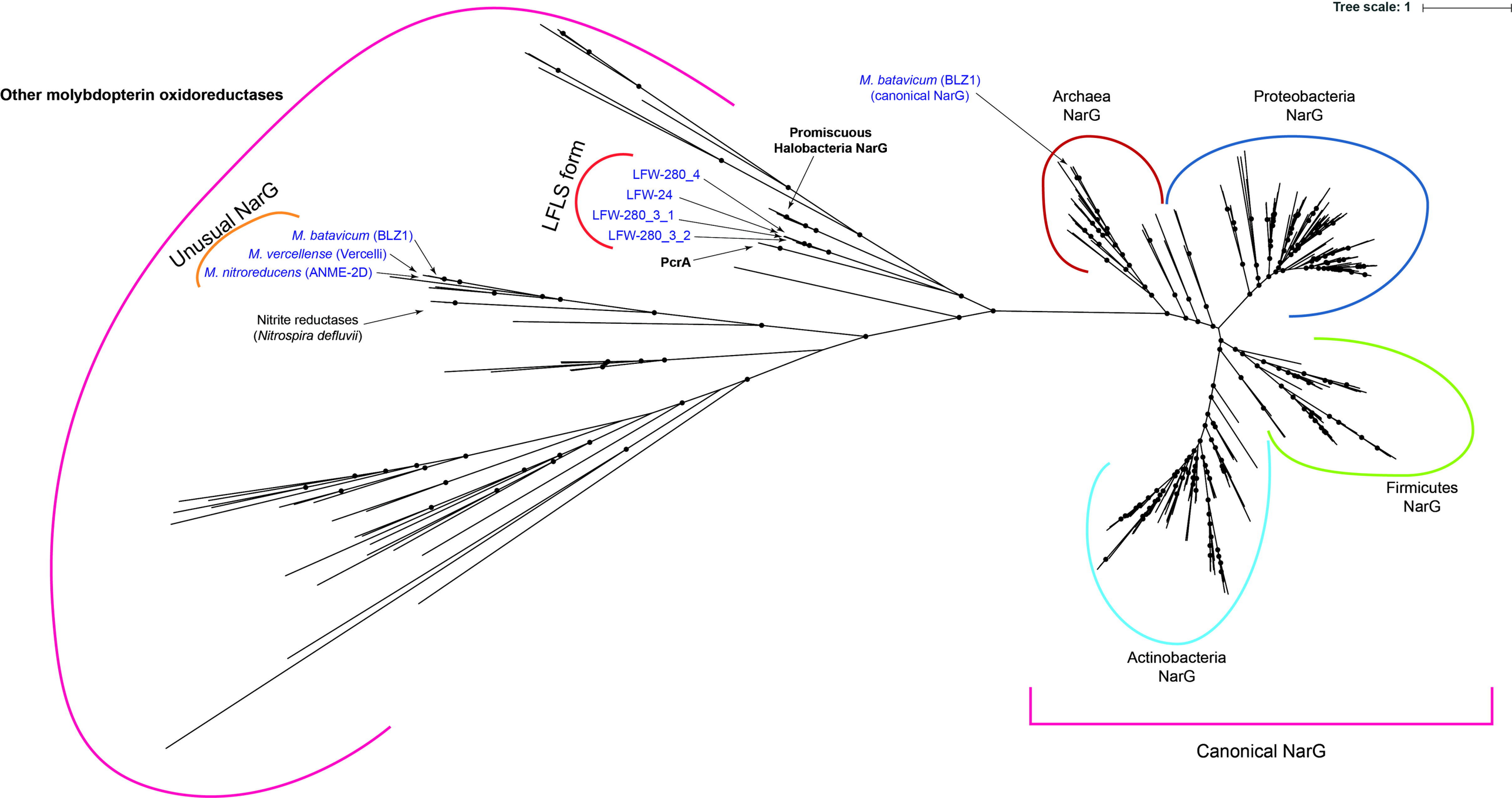
Tree scale: 1
Other molybdopterin oxidoreductases
Unusual NarG
M. batavicum (BLZ1)
M. vercellense (Vercelli)
M. nitroreducens (ANME-2D)
Nitrite reductases
(Nitrospira defluvii)
LFLS form
LFW-280_4
LFW-24
LFW-280_3_1
LFW-280_3_2
PcrA
Promiscuous
Halobacteria NarG
M. batavicum (BLZ1)
(canonical NarG)
Archaea
NarG
Proteobacteria
NarG
Firmicutes
NarG
Actinobacteria
NarG
Canonical NarG